Canonical Host-Pathogen Trade-Offs Subverted by Mutations with Dual Benefits

Robert Beardmore,[1,*] Mark Hewlett,[1] Rafael Peña-Miller,[2] Ivana Gudelj,[1] and Justin R. Meyer[3,*]

1. Biosciences, Geoffrey Pope, University of Exeter, Stocker Road, Exeter EX4 4QD, United Kingdom; 2. Centro de Ciencias Genómicas, Avenida Universidad s/n, Colina Chamilpa, CP 62210, Cuernavaca, Morelos, Mexico; 3. School of Biological Sciences, University of California, San Diego, La Jolla, California 92093

Submitted October 7, 2021; Accepted August 24, 2022; Electronically published April 10, 2023

Online enhancements: supplemental PDF.

ABSTRACT: Host-parasite coevolution is expected to drive the evolution of genetic diversity because the traits used in arms races—namely, host range and parasite resistance—are hypothesized to trade off with traits used in resource competition. We therefore tested data for several trade-offs among 93 isolates of bacteriophage λ and 51 *Escherichia coli* genotypes that coevolved during a laboratory experiment. Surprisingly, we found multiple trade-ups (positive trait correlations) but little evidence of several canonical trade-offs. For example, some bacterial genotypes evaded a trade-off between phage resistance and absolute fitness, instead evolving simultaneous improvements in both traits. This was surprising because our experimental design was predicted to expose resistance-fitness trade-offs by culturing *E. coli* in a medium where the phage receptor, LamB, is also used for nutrient acquisition. On reflection, LamB mediates not one but many trade-offs, allowing for more complex trait interactions than just pairwise trade-offs. Here, we report that mathematical reasoning and laboratory data highlight how trade-ups should exist whenever an evolutionary system exhibits multiple interacting trade-offs. Does this mean that coevolution should not promote genetic diversity? No, quite the contrary. We deduce that whenever positive trait correlations are observed in multidimensional traits, other traits may trade off and so provide the right circumstances for diversity maintenance. Overall, this study reveals that there are predictive limits when data account only for pairwise trait correlations, and it argues that a wider range of circumstances than previously anticipated can promote genetic and species diversity.

Keywords: host-pathogen coevolution, life history trade-offs.

* Corresponding authors; email: r.e.beardmore@exeter.ac.uk, jrmeyer@ucsd.edu.

ORCIDs: Beardmore, https://orcid.org/0000-0003-1770-1009; Hewlett, https://orcid.org/0000-0001-8628-3897; Peña-Miller, https://orcid.org/0000-0002-2767-0640; Ivana Gudelj, https://orcid.org/0000-0003-3450-6854; Meyer, https://orcid.org/0000-0001-5566-8452.

Introduction

Phages and Costs of Resistance

Many different theoretical frameworks are consistent in their prediction that when improvements in one trait incur costs in a second trait, then natural selection can drive the evolution and maintenance of genetic and species diversity (Metz et al. 1996; Gudelj et al. 2006; Mealor and Boots 2006; Meyer et al. 2015). While empirical and theoretical studies have focused on trait pairs to test this idea, less attention has been paid to correlations between three or more traits, yet this is said to be crucial to our understanding of how microbial communities function (Lindsay et al. 2021). This gap in our understanding is particularly problematic because multitrait interactions are hard to reconcile with theories derived from two-trait trade-offs. This is because it is logically impossible that three traits engage in simultaneous, mutual trade-offs: logic dictates that if trait X trades off with Y and Y trades off with Z, then X and Z will necessarily "trade up" (i.e., X and Z are positively correlated). Given this and the observation that traits do not evolve as pairs in isolation but rather within complex organisms, we seek insights into multitrait trade-off relationships.

We therefore studied a tractable two-species laboratory system: the bacterium *Escherichia coli* B(REL606) and one of its viruses, bacteriophage λ. We selected these because their molecular interactions are well understood, allowing for careful experimental controls, and a large number of analytical tools are available for interpreting experimental outcomes. These organisms are also amenable to the generation of libraries of genetic variants that can be used to test trade-off theories, and within days of coculture, here we see *E. coli*-λ coevolution yield genetically distinct bacterial variants that differ in key resistance and host range traits that

are predicted to trade off with other aspects of reproduction. This permits the rapid generation of genotypes that vary significantly in phenotypes that fall at varying positions in trait space.

This system was also studied because the trade-offs intrinsic to phages and bacteria have important clinical implications. The World Health Organization predicts that the next 30 years will see more people die from antibiotic-resistant bacterial infections than from cancer (Interagency Coordination Group on Antimicrobial Resistance 2019), although this prediction could be overstated (de Kraker et al. 2016; Baquero 2021). Nevertheless, a search for alternative treatments has revived phages as an antibacterial therapeutic (Summers 2001; Miedzybrodzki et al. 2012; Rohde et al. 2018; Petrovic Fabijan et al. 2020) for which trade-off theory makes important predictions: trade-offs that secure permanent fitness costs of phage resistance will help maintain the utility of phage therapy. However, this was already said for costs of antibiotics that can fail because costs either do not materialize (Borghi et al. 2014) or are compensated by additional mutations (Sandegren and Andersson 2009; Andersson and Hughes 2010). Much worse than a lack of costs would be a scenario where phage resistance brings with it an increase in bacterial fitness; we call this a "trade-up." Given this and the strength of selection for phage resistance, resistant genotypes would likely sweep the population and lead to untreatable infections with increased capacity to reproduce and greater virulence. Moreover, mutations with trade-ups have been observed in phage-bacterial interactions (Andrews and Fields 2020; Burmeister et al. 2020).

We therefore set out to systematically quantify a number of bacterial and phage life history traits that evolve during coevolution and to understand how trait values correlate. We focused on three trade-offs. The first is the host range trade-off (HRTO): infection by parasites is a known driver of genetic diversity, and this parasitism trade-off is central to our understanding of how parasites target their hosts. HRTO theory postulates that if a parasite is efficient at targeting one host, it will be inefficient at targeting others (Agrawal and Lively 2002; Forde et al. 2008; Weitz et al. 2013). The second is the cost of resistance trade-off (CORTO): trade-offs play a role in phage therapy, for if a pathogenic bacterium evolves to evade all of the phages that it is currently susceptible to, that bacterium will no longer be treatable therapeutically by phages. However, a postulated CORTO (Hall et al. 2012) whereby increases in phage resistance incur reductions in bacterial growth rate suggests that such highly resistant bacteria, which can be observed in patients (Rohde et al. 2018), will be poor replicators. Third, we study the rate-yield trade-off (RYTO), where slower-growing bacteria are more efficient at producing biomass per available nutrient, a trait known as "biomass yield" (Meyer et al. 2015).

We observed a within-strain RYTO for almost all bacterial variants, but the main finding is this: the totality of data we generated contains of thousands of trait measurements, but it exhibits little trade-off data. We observed no robust between-strain RYTO and no CORTO, and a trade-up appeared where we had expected to find an HRTO. The remainder therefore discusses a multitrait trade-off theory that provides a mechanistic understanding of the absence of trade-offs and assesses the implications of our data for microbial diversity and phage therapy.

Algebra of Multiple Traits: Two-Trait Trade-Offs Yield Trade-Ups

To create genetic variants, we cultured *E. coli* and λ under conditions where a trade-off between bacterial growth and phage resistance was expected (see "Methods"). Bacteriophage λ uses the *E. coli* outer membrane protein LamB as a receptor, and *E. coli* mutations in this protein can confer resistance to λ (Thirion and Hofnung 1972; Hofnung et al. 1976). *Escherichia coli* also uses LamB to transport maltodextrins, and LamB mediates other functions too, as discussed below. By culturing *E. coli* in growth medium where maltodextrins are the limiting resource, we expected that λ-resistant mutants would pay a fitness cost for their ability to grow. However, this prediction did not materialize, and instead we observed fitness-resistance trade-ups in some mutants. This unexpected observation led us to develop theory to help identify which assumptions led to our faulty prediction, leading to new insights into multitrait interactions.

The fact that one protein can mediate many traits can be problematic for the generalizability of two-trait trade-off theory. Here, LamB mediates several trade-offs (fig. 1): self-preservation and nutritional competence (SPANC) balance (Ferenci 2005), the RYTO (Pfeiffer and Bonhoeffer 2002; MacLean and Gudelj 2006; Novak et al. 2006; Maharjan et al. 2007; Lipson et al. 2009), CORTOs (Sanchez 2011), the rate-affinity trade-off (Gudelj et al. 2007; Meyer et al. 2015), and the HRTO (Weitz et al. 2005; Forde et al. 2008). So we asked this: what would theory predict if a third trait depends in a functional, mechanistic manner on two other traits that are already known to trade off with each other?

To address this, consider an idealized context whereby quantitative traits X and Y are traded mathematically, so assume $X = f(Y)$, where $f(\cdot)$ represents a one-dimensional trait relationship that is decreasing: $f(Y_1) > f(Y_2)$ whenever $Y_1 < Y_2$. Thus, if f is a smooth function, it has negative derivative df/dY. Now assume traits Y and Z are also traded: $Y = g(Z)$, where g is a decreasing function. This places a constraint on how X and Z can interact—$X = f(g(Z))$—and elementary calculus implies

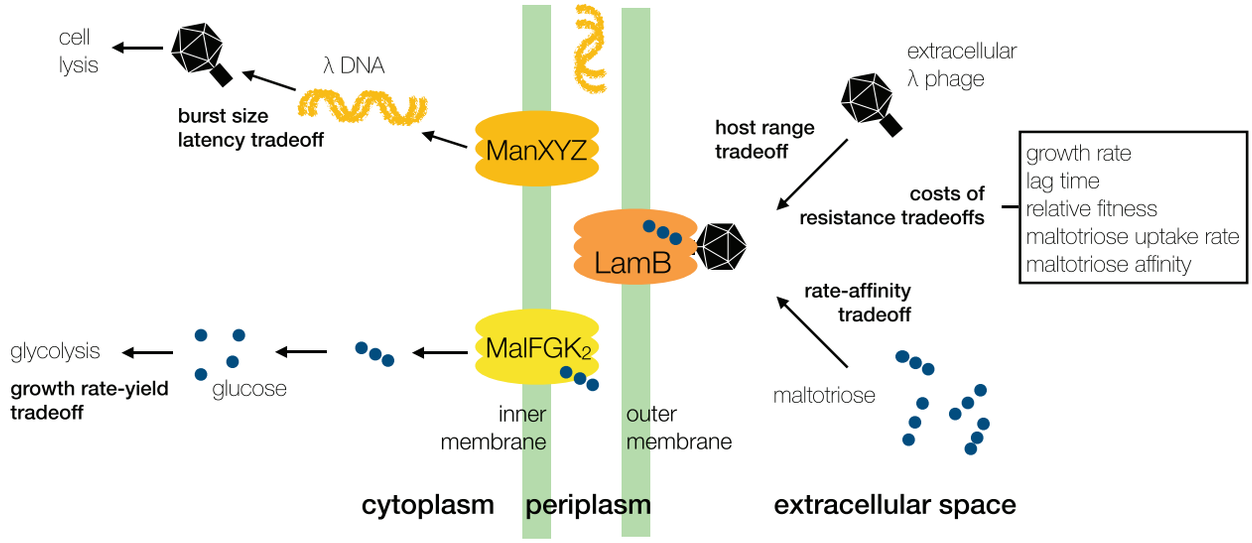

Figure 1: The membrane protein LamB is a virus receptor and maltoporin transporter, thus a bottleneck for many trade-offs. Both extracellular maltotriose and phage λ DNA enter *Escherichia coli* by first passing through the LamB maltoporin, so λ resistance and maltotriose uptake rates and affinities are codependent, which could create fitness costs of resistance. Moreover, nutrient transporters exhibit biophysical rate-affinity trade-offs by virtue of their function: transporters with higher affinities cannot translocate their substrates as quickly. A host range trade-off could also arise whereby λ's tail binds preferentially to certain LamB structures but binds suboptimally to other structures. Interactions are complicated further by a branching of trade-offs whereby phage DNA traverses the inner membrane through a different transporter (ManXYZ) to maltotriose (MalFGK). Once inside the cell, maltotriose produces glucose, and metabolic trade-offs could then ensue whereby slower glycolytic pathways are more adenosine triphosphate efficient. And as it takes less time to assemble fewer virions, a latency trade-off could arise for viruses with smaller burst sizes. As a result of λ biology, these processes place several trade-offs downstream of each other in a serial and a parallel arrangement that forms an X-shaped topology.

$$\frac{dX}{dZ} = \frac{df}{dY}(g(Z)) \cdot \frac{dg}{dZ}(Z). \tag{1}$$

The signs of the derivatives in equation (1) ensure that dX/dZ is positive because it is the product of two negative quantities; thus, X and Z engage in a trade-up. For this reason, trade-off relationships are not transitive between trait pairs, but trade-ups (i.e., the functional relationship $f(g)$ between X and Z here) are.

Extending this rationale, we reason that a biological system harboring n idealized trade-offs could also exhibit $n(n-1)/2$ trade-ups. To see this, assume that n traits trade off with some trait A. There are

$$^{n+1}C_2 = n(n+1)/2$$

trait pairings in total, of which n are trade-offs; thus, the remaining $n(n+1)/2 - n = n(n-1)/2$ trait pairs must form trade-ups (because all of those traits trade off with A). We deduce that if $n > 4$ traits trade off with A, because $n(n-1)/2 > n$ there are more trade-ups than trade-offs; table 1 illustrates cases $n = 3, 4, 5$. We note that this analysis is not exhaustive because other trade-off tables could exist than the parity structure indicated in table 1.

The logic of table 1 simplistically assumes that trait interactions are pairwise and cannot be mediated by a third trait. This restriction is unlikely to apply in practice, where trait relationships can be mediated by many exogenous factors, both environmental and genetic, so we now illustrate how the above-described logic extends to a more realistic biological context, motivated by LamB mutants of *E. coli*.

Algebra of Multiple Traits: A Detailed Theoretical Example

To better understand table 1, we now present a mechanistic rationale whereby two traits, A and B, trade off and so too

Table 1: Parity relationships when different numbers of traits (A–E) exhibit trade-offs

	Three traits		Four traits			Five traits			
	B	C	B	C	D	B	C	D	E
A	−1	−1	−1	−1	−1	−1	−1	−1	−1
B		+1		+1	+1		+1	+1	+1
C					+1			+1	+1
D									+1

Note: According to equation (1), there should be parity relationships between trade-offs, and some are shown here: trade-offs (denoted by −1) are more common than trade-ups (denoted by +1) when three traits are considered, but when five traits or more are considered, trade-ups are more common.

do A and C, yet B and C have a positively related functional dependence. We achieve this by arguing that certain environmental conditions can support increased phage resistance (this will be trait A) among bacterial cells with higher absolute fitness (also known as growth rate; trait B) because of changes in those cells' nutrient acquisition properties (trait C). This rationale will show that fitness costs of phage resistance (the CORTO) need not materialize in practice because there are metabolic routes to fitness benefits that accrue when phage resistance increases.

The argument starts thus: the LamB protein is both a maltotriose transporter and a λ receptor. So, suppose a structural mutation in the *lamB* gene located in the *mal* operon occurs in an ancestral (also known as wild type) phage-susceptible bacterial strain. Suppose this mutation hampers phage binding and renders the mutantless phage susceptible. There follow two possible nontrivial side effects: this mutation either (i) hastens maltotriose uptake or (ii) slows maltotriose uptake. In case i, for which mutations have been observed (Andrews and Fields 2020), this could incur no cost of resistance because increased nutrient uptake could also increase growth rate, bestowing a dual benefit on the bacterium. However, these mutations appear to be rare, and instead most mutations that cause resistance also slow maltotriose uptake, either by lowering maltotriose affinity for LamB or by reducing the maltotriose translocation rate through LamB, as per case ii (Andrews and Fields 2020).

Now, mutations in case ii would, by virtue of decreasing nutrient uptake, seem deleterious for the mutant because they reduce intracellular nutrient concentration, creating a cost of resistance because these nutrients are used for biomass production. However, the consideration of functionally related traits is important here: once inside the cell, downstream metabolism is impacted by different rates of flux of nutrients that can produce unintuitive growth responses. For example, glucose metabolism (glycolysis) can exhibit an RYTO whereby a slowing of adenosine triphosphate (ATP) production by reduced nutrient uptake can improve ATP production efficiency (MacLean and Gudelj 2006; Meyer et al. 2015; Reding-Roman et al. 2017). As maltotriose is degraded by protein products of *mal* into glucose, it may therefore experience efficiency increases that could potentially benefit absolute fitness.

At this point, table 1 is relevant because this argument invokes two trade-offs, one downstream of the other, to form a trade-up. Details of the argument will depend crucially on the relative strengths of all of the traits and trade-offs involved, but we postulate that the following could happen. On one hand, slower maltotriose uptake through a mutant LamB could quite reasonably incur a fitness cost of resistance, but on the other hand, it need not do so because if circumstances see slower nutrient uptake lead to a lower rate of glycolytic metabolism, this can lead to a concomitant increase in glycolytic efficiency (measured in ATP produced per substrate processed; MacLean and Gudelj 2006). If this efficiency gain is sufficiently large, cellular growth rate could then increase. Thus, while there might be a cost of resistance in terms of reduced nutrient uptake, there is no cost in terms of the derived absolute fitness, and there may even be a benefit.

We can formalize this verbal argument mathematically as follows. Write cellular growth rate, $G(S; V)$, as a nonlinear function of the extracellular nutrient concentration (maltotriose, S) that plateaus at the maximum growth rate, just as Jacques Monod described:

$$\begin{aligned} G(S; V) &= \overbrace{\text{nutrient-to-biomas conversion}}^{\text{biomass yield/conversion efficiency}} \\ &\quad \times \text{nutrient uptake rate} \\ &= c(S_i)\frac{VS}{K_m + S}. \end{aligned} \tag{2}$$

Here, mutable trait V is a maximal maltotriose uptake rate phenotype, K_m is a half-saturation phenotype, and $c(S_i)$ is biomass yield measured per intracellular maltotriose, S_i, where S_i depends on extracellular maltotriose S. Decreasing functions are appropriate (Meyer et al. 2015) for $c(S_i)$, for instance if we assume $S_i \approx S$, in which case the theoretical form

$$c(S_i) \approx c_{\text{hi}}\frac{1}{1 + pS_i} + \frac{\text{p}S_i}{1 + \text{p}S_i}c_{\text{lo}} \tag{3}$$

can be derived using elementary properties of branched metabolic pathways with different ATP yield efficiencies on each branch (Meyer et al. 2015).

Here, c_{hi} and c_{lo} are maltotriose-to-biomass conversion efficiencies, respectively, the low-maltotriose and high-maltotriose asymptotes in biomass yield that cells can achieve, where $c_{\text{hi}} > c_{\text{lo}} > 0$. The function $c(S_i)$ is a "within-strain" RYTO, and accordingly $dc/dS_i < 0$, meaning that increased maltotriose concentration reduces biomass yield and the variable $p > 0$ controls trade-off "strength." A within-strain RYTO here means that as nutrient supply increases, so too does growth rate, but the strain will produce less biomass per unit of nutrient supplied. There is no particular biological reason to use model (3), and the function $c(S_i) = c_{\text{hi}}\exp(-pS_i)$ will be used below because it vastly simplifies several theoretical calculations.

Now, there are many possible models that relate extracellular and intracellular sugars to each other, so S_i to S, each assuming different biophysical properties of the cell. One could suppose cell volume is constant, for simplicity; set $D > 0$ to be a nutrient diffusion rate in and out of the cell, and let m be the rate at which S_i is enzymatically degraded. We could then write

$$\frac{d}{dt}S_i = D(S - S_i) + \frac{VS}{K_m + S} - mS_i, \tag{4}$$

and assuming equation (4) to be in equilibrium, it relates S_i to S uniquely: $S_i = DS/(m + D) + VS/(m + D)(K_m + S)$. The latter relation can be inverted so that the external nutrient concentration can be inferred from the intracellular nutrient concentration, $S = S(S_i; V, K_m)$, which has the consequence of rendering biomass efficiency a function of extracellular nutrient concentration, namely, $c(S_i) = c(S_i(S; V, K_m))$.

Returning to case ii of the verbal argument given above, now suppose a mutation that reduces the binding affinity of λ phage to LamB also decreases the maximal maltotriose uptake rate, which is V. Denoting the change in V by $dV < 0$, we ask this: are there any circumstances under which $G(S; V)$ increases for some values of S when V decreases? If the answer to this is affirmative, then, paradoxically, absolute fitness will increase in some environmental conditions if phage resistance brings about a reduction in maltotriose uptake. Mathematically, for this to happen we require

$$\frac{\partial G}{\partial V} < 0 \quad \text{for } dV < 0,$$

as then

$$\begin{aligned} G(S; V + dV) &= G(S; V) + \overbrace{\frac{\partial G}{\partial V}(S, V) \cdot dV}^{- \times - = +} + O(dV^2) \\ &> G(S; V), \end{aligned} \tag{5}$$

provided dV is sufficiently small in size and negative. Equation (5) follows by Taylor's theorem from elementary calculus, which states that functions of dV can be approximated by power series in dV.

To determine the sign of $\partial G/\partial V$, write the uptake function $U \coloneqq VS/(K + S)$ so $\partial U/\partial V = U/V$ and use a prime symbol (′) to denote an ordinary derivative. From elementary calculus

$$\begin{aligned} \frac{\partial G}{\partial V} &= \frac{\partial}{\partial V}(c(S_i) \cdot U) \\ &= c'(S_i)\frac{\partial S_i}{\partial V} \cdot U + c(S_i) \cdot \frac{\partial U}{\partial V} \\ &= \frac{U}{V} \cdot c'(S_i) \cdot \left(V \overbrace{\frac{\partial S_i}{\partial V} + \frac{c(S_i)}{c'(S_i)}}^{Q(S) \coloneqq} \right), \end{aligned}$$

and this expression is negative when the bracketed term is positive because $U, V > 0$ and $c'(S_i) < 0$. It is so important we define the bracketed expression as a function in its own right:

$$Q(S) \coloneqq V\frac{\partial S_i}{\partial V} + \frac{c(S_i)}{c'(S_i)}. \tag{6}$$

The condition $Q(S) > 0$ applied to definition (6) formalizes a requirement on the environment and the strength of the RYTO needed to produce growth rate increases when nutrient acquisition is impaired by a phage-resistance mutation.

To tailor this calculation to a particular circumstance, let $c(S_i) = c_{\text{hi}} \exp(-pS_i)$ and consider definition (6). In this case, the algebra is much simplified relative to using model (3), and then

$$Q(S) = \frac{VS}{(m + D)(K_m + S)} - \frac{1}{p}. \tag{7}$$

In this case, Q is a scaled and shifted Monod function. Straightforward algebra shows that $Q(S)$ changes sign once at a critical value of S, passing from negative to positive as S increases provided the RYTO is strong enough (i.e., $p > (m + D)/V$). Hence, there are two zones of nutrient concentration, S, based on the signs of $Q(S)$ situated at high and low S, which delineate positive and "negative" fitness costs of phage resistance.

Thus, we predict that absolute fitness of a bacterium can increase when nutrient uptake rate decreases provided the RYTO is present and the extracellular environment is sufficiently nutrient rich. We also predict that fitness can decrease when uptake rate decreases due to an analogous mutation if the extracellular environment is sufficiently nutrient poor.

This analysis can be extended (we omit the mathematical details, and calculations are possible but more arduous if model [3] is used), although its scope is limited due to its biological assumptions and so other possibilities exist whereby trade-offs and fitness costs may not be observed when resistance to phage evolves. It is, for example, feasible that compensatory mutations quickly mitigate fitness costs that were present at some point but that are not detected in practice because the compensated genotypes fix too quickly. The latter could occur within LamB itself or else in a downstream glycolytic mutation that increases nutrient-biomass conversion efficiency, which might compensate for reductions in nutrient uptake. Moreover, missense mutations have been identified in LamB where phage binding is impaired relative to an ancestral strain yet maltodextrin uptake is maintained or improved, although deep mutational scanning shows that these are likely rare (Andrews and Fields 2020). More trivial possibilities exist too; for instance, LamB expression is not needed for cell growth if no maltodextrin is present in the extracellular environment, and in that case down-regulation of the *mal* operon or loss-of-function mutations in *mal* can render cells resistant to λ with no fitness cost at all (Borin et al. 2021). These possibilities sit outside the context of the above-described theory, which addresses a nontrivial context in which two trade-offs can conspire to create a

trade-up of fitness benefits, just as table 1 predicts in a manner free of biological context.

Methods

We now seek data to test our theory using a library of laboratory phage and bacterial variants with different growth rates and resistance phenotypes to test whether data are consistent or in conflict with theory. Those data will also be used to test for the presence of several trade-offs (Kraaijeveld and Godfray 1997; Bohannan et al. 2002; Ferenci 2005; Lipson et al. 2009; Molenaar et al. 2009; Beardmore et al. 2011; Poelwijk et al. 2011; Aktipis et al. 2013; Keen 2014).

Phage and Bacterial Mutant Library Generation

To create a library of phage and bacterial variants, we cocultured *Escherichia coli* strain B(REL606) with the obligately lytic λ phage strain cI26. When cocultured with cI26, REL606 experiences pressure to evolve resistance because *E. coli* B strains lack generalized phage defenses, such as mucoid cell formation, restriction modification, or CRISPR adaptive immunity (Spanakis and Horne 1987; Daegelen et al. 2009). This pressure is magnified by the lytic phage's increased virulence compared with its lysogenic relatives (Lenski 1988). Once *E. coli* evolve resistance, phages typically experience selection to evolve a counterattack, triggering a rapid arms race within few generations.

Thus, 100 flasks were initiated with phages (~10^2 particles) and 10^3 bacterial cells that were preconditioned in the experimental environment for 24 h. These small initial populations were used to increase the likelihood that mutations for defense and counterdefense would arise de novo, increasing the likelihood of isolating unique *lamB* mutations and evolving divergent phage genotypes between replicates. Flasks were filled with 10 mL of modified Davis medium (DM; Lenski et al. 1991; 125 μg/mL maltotriose instead of glucose and 1 μg/mL magnesium sulphate). Bacteria and phages were allowed to reproduce for 24 h at 37°C and shaken at 120 rpm. At 24 h, a 100-μL random sample of each flask was added to a fresh flask, and the bacteria and phage populations were allowed to grow again. This cycle was repeated once more, and phages and bacteria were sampled after the third day of growth. We terminated the experiment at this early time point to try to ensure that bacteria would acquire a small number of mutations so as to simplify the relationships between genotypes and phenotypes, avoiding compensatory or other types of mutations that could have confounding effects. Moreover, a prior study observed the greatest genotypic diversity on day 3 (Meyer and Lenski 2019). We show below that *E. coli* evolve resistance in this assay through several loci, the most common of which is *lamB*.

Bacterial and Phage Isolation and Storage Procedures

To isolate mutant bacteria, we streaked liquid samples on Luria-Bertani (LB) agar plates (Sambrook and Russell 2001), randomly picked two colonies, and then replated two more times to remove all phages. Finally, we grew each colony in liquid LB medium overnight and preserved two 1-mL samples in 15% glycerol, frozen at −80°C. The entire phage population for each flask was preserved by chloroform preparation of the remaining volume of culture, 8 mL (Adams 1959). Clonal isolates of the phages were created by picking plaques (miniature epidemics derived from a single phage particle) from bacterial lawns (films of bacteria immobilized in soft agar spread on top of petri dishes (Adams 1959). For each phage population, we attempted to isolate phages from three separate lawns, one derived from the ancestral bacteria (REL606) and the two bacteria isolated from the very same flask. By using the coevolved bacteria or phage isolation, we reasoned that this increased the likelihood of sampling phages that had evolved specialized local interactions with their coevolved bacteria, thereby improving the likelihood of uncovering more phage diversity with modular bacteria-phage interactions than if we had used only ancestral bacteria. Two plaques from each flask were isolated and clonal cultures were created according to Adams (1959). When choosing phages, plaques were favored that formed on the lawns of the coevolved bacteria.

This procedure yielded more bacteria than appear in this study, and a bacterial isolate was removed if it showed identical levels of resistance to another isolate from the same flask. Thereafter, bacteria were removed if they did not possess a *lamB* mutation. This left 50 mutant strains and the ancestral strain to form the study library of 51 bacteria; it also left 93 phages. All of these strains were sent from the US laboratory (University of California, San Diego) to a collaborating UK laboratory (Exeter University) for analysis, but only 46 bacteria could be cultured in the different lab conditions. This left some missing data; for instance, five strains (20b, 52a, 65b, 67a, 96a) had infectivity phenotypes but no growth rate data and vice versa for two strains (8a, 14a), leaving 44 strains with both those data types intact.

Estimating Bacterial Resistance to a Library of Phages

We measured λ resistance by challenging every isolated bacterium with every phage isolate (fig. 2). To do this, we made spot plates by dripping ~2.5 μL of each phage stock (between half a million to 1 million phage particles) on bacterial lawns (Adams 1959). After 24 h of growth at 37°C, the bacterial lawn would thicken unless a phage was able to lyse it, in which case a round clearing (spot) formed under the drip. Digital images were taken of each plate using an AlphaImager 2200 (Alpha Innotech). Data for the matrix

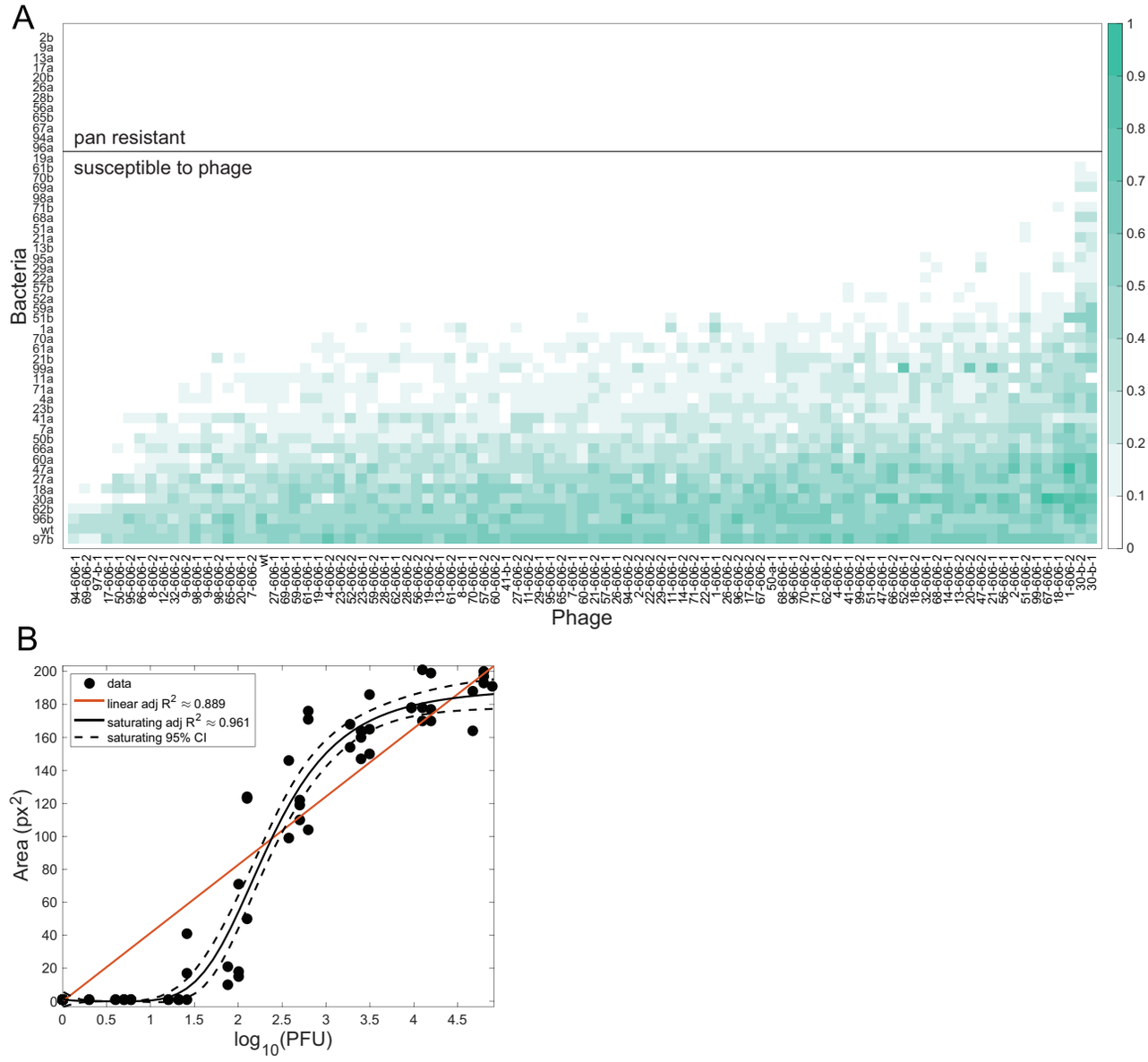

Figure 2: *Escherichia coli* susceptibility to λ was quantified by analyzing images of phage clearing on bacterial lawns (of 51 bacterial strains, 12 are panresistant, noting that strain 19a is not). *A*, This infectivity matrix is the result of applying a blob-based imaging procedure (see fig. S1) in which the blob area represents phage infectivity. This matrix represents the infectivities of the entire bacteria and phage libraries after having sorted rows and columns, and it appears to be banded, exhibiting no blocked submatrices within its structure. A statistical analysis makes this precise; by seeking modular subnetworks of interacting phage and bacterial clusters one can show that the matrix has no isolated interacting submodules and, instead, has a graded structure (see fig. S2, where matrix entries are normalized so as to lie between 0 and 1). *B*, We validate the quantitative imaging approach from *A* by comparing a traditional phage counting method with these imaging data: plaque-forming units (PFUs) and image blob area (pixels^2 are positively correlated over three orders of magnitude via a slowly saturating nonlinearity; eq. [8]). CI = confidence interval.

of interactions used here was previously reported qualitatively where clearings were determined by eye and a 0 or 1 was recorded for whether or not a given phage infected a given bacterium (Flores et al. 2011). Here, we used an image analysis procedure described later to quantify the infectivity of each phage to each bacterium. These spot plates were repeated twice and yielded similar qualitative results, but image analysis–based quantification was performed only on the second set after our techniques had improved. We then validated this procedure by varying the density of

cI26 and spotting on the sensitive bacteria. In total, 56 spots with phages and 40 negative control spots were analyzed. Next, we estimated phage density by counting plaque-forming units (PFUs) and tested whether there was a monotonic relationship between PFUs and the spot size, something we found using the shifted Hill function:

$$A(x) = \frac{p_2|x - p_3|^{p_1}}{p_4 + |x - p_3|^{p_1}}, \quad (8)$$

where A is one more than the area of the imaged spot (pixels^2), x represents log(1 + PFUs), and each parameter p_j was determined using a data-fitting procedure implemented in Matlab (fig. 2*B*).

Growth Assays

To estimate growth rate, biomass yield, and other growth parameters of each LamB variant, we monitored the growth of each *E. coli* isolate in microtiter plates using a Tecan M200 Infinite Pro. Each strain was cultured in DM with varying concentrations of maltotriose (2.5, 5, 10, 20, 40, 80, 160, and 250 μg/mL). Before growth was measured, cells were revived from the freezer in 4 mL of liquid LB medium at 37°C, shaken at 160 rpm, and grown overnight. The next day, 10 μL of the culture was propagated in DM with 125 μg/mL maltotriose and grown for 24 h. This step was repeated for one additional day to acclimate the cells to experimental growth conditions. Approximately 100 cells were inoculated into each well filled with 200 μL of DM. Cultures were incubated at 37°C, optical density (OD) at wavelength 600 nm was read every 20 min, and the plates were shaken before each reading to suspend the cells and oxygenate the cultures. Experiments lasted until all isolates reached carrying capacity, typically at about 18 h, although some cultures did not reach carrying capacity. Wells on the edge of the plate were not used to measure changes in OD, and the experiment was batched so that every isolate was cultured on each plate and maltotriose concentration varied between batches.

When stationary phase is achieved during a growth assay, yield can be determined by dividing population density by the maltotriose concentration (Meyer et al. 2015). We state yield in units of OD per microgram per milliliter throughout, but this can be converted into natural units of cells per microgram using the fact that growth assays were conducted in 200-μL volumes and 1 OD $\approx 7.6 \times 10^8$ cells in our culture conditions (Meyer et al. 2015).

Competitive Ability Assays

Competitive fitnesses of the bacterial library mutants were measured by competing each genotype "head to head" with a genetically marked version of the ancestor, REL607. REL607 (ara$^+$) can metabolize arabinose whereas REL606 (ara$^-$) cannot because of a single nucleotide substitution that has little effect on bacterial fitness in our culture conditions. Marked and unmarked genotypes can be distinguished on tetrazolium arabinose plates, which provides a tool for estimating the relative frequency of each in a mixed population. Full descriptions of these competition experiments can be found elsewhere (Lenski et al. 1991; Travisano et al. 1995), but to summarize we initiated each flask with 50% of the resistant type and 50% of its ara$^+$ ancestor. We cultured them for 3 days, as per the above-described coevolution experiment, and then measured their initial and final densities and calculated the ratio of the Malthusian parameters for the evolved strain versus the ancestor. We performed three replicates for each *lamB* variant.

Sequencing

We sequenced *lamB* for at least one bacterial isolate from each flask, and a second isolate was sequenced if preliminary tests revealed that the two sympatric isolates had different levels of phage resistance. Sequencing was performed with an automated ABI sequencer maintained at the Michigan State University Research Technology Support Facility. Polymerase chain reaction–amplified fragments purified with GFX columns were used as templates. Fragments were amplified with primer sequences 5′-TTCCCG GTAATGTGGAGATGC-3′ and 5′-AATGTTTGCCGGG ACGCTGTA-3′, placed 1,398 bases upstream and 504 bases downstream of the gene, respectively.

Of all the variants isolated, full genomes of 13 *E. coli lamB* mutants were sequenced to test whether the bacteria evolved more than a single mutation for resistance and whether other mutations may have impacted *E. coli lamB* growth. Isolates that we suspected had multiple λ-resistant mutations were chosen because they evolved high levels of resistance despite only possessing a single amino acid change in LamB, because a mutation in *lamB* was not discovered, or because the genotype possessed a distinct resistance profile. Technicians at the Research Technology Support Facility at Michigan State University sequenced the genomes using an Illumina Genome Analyzer IIx. Genomic DNA samples were created by reviving frozen bacteria in LB medium, growing them overnight, and then isolating DNA from several milliliters of the culture with Qiagen genome tips. Samples were fragmented by sonification, prepared with bar-coded attachments, and multiplexed over four lanes. Mutations were predicted from the resulting 75-base DNA single end reads using breseq (ver. 0.13; https://www.sanger.ac.uk/science/tools/ssaha2-0) and the ancestral genome (GenBank accession number NC_012967.1) used as the reference.

Protein Shape Prediction from Amino Acid Sequence

Mutant LamB protein structures were predicted for each variant using Modeller (http://salilab.org/modeller/). Predictions were made in two steps. First, homology-based techniques were used to generate a protein structure by using the known ancestral LamB shape as a guide; LamB structure was then determined by X-ray crystallography to 3.10-Å resolution (Schirmer et al. 1995; GenBank accession number YP_003047080). Next, de novo loop refinement reorganized protein conformation to minimize entropy created by electrostatic conflicts introduced by the substituted amino acid.

Results

Testing for an HRTO Using Imaging Analysis (Figs. 2, 3)

Having generated a library of phages and bacteria, we tested for nonrandom patterns in the interaction network between the two (Flores et al. 2011, 2013, 2016; Weitz et al. 2013; see especially fig. 3 in Flores et al. 2013) as a first step toward designing a test for the HRTO. One can determine such a network from two sets of N bacteria and M phages by calculating an infection matrix, which is an $N \times M$ array of likelihoods that bacterial genotype i is infected by phage genotype j on contact (Werts et al. 1994; Flores et al. 2013). To obtain proxies for these likelihoods, where traits are called "infectivities" for phages and "susceptibilities" for bacteria, we performed infection assays (see "Methods") on N bacterial lawns, one lawn per bacterium, each inoculated with all M phages. Finally, infectivities and susceptibilities were quantified using imaging algorithms (fig. S1) to produce an infectivity matrix, Φ (fig. 2*A*). Note how some library phages are able to infect none of the bacteria; we call these "panresistant" bacteria.

The numerical structure of the infectivity matrix, Φ, can be used to test the idea that phages and bacteria cluster into highly interacting functional subunits. For instance, some phage subgroups could be highly infectious to a subgroup of bacteria without infecting other bacteria not in that group. If multiple such groupings were present in data, this would be evidence of modularity, and Φ would look approximately "block structured." For instance, a matching-alleles infection mechanism would provide an example of a modular structure (Agrawal and Lively 2002). However, our bacteria and phage strains provide no statistical support for this because Φ is better described as having a graded, or nested, structure (this is apparent from a visual inspection of Φ; fig. 2*A*; fig. S2 supports this with statistics). These data exhibit a grading that ranges from low-infectious to highly infectious phages and a second grading that ranges from low-resistant to highly resistant bacteria. We asked why such a structure would describe bacteria-phage infectivities, and a biophysical study of LamB mutants provides some insights into this, as described in "Adaptation Hot Spots in LamB Structure" below.

The nested infection matrix, Φ, provides a convenient method for testing the HRTO that modular networks do not afford. In a nested infection matrix, the phage with the narrowest host range infects hosts that are a subgroup within the larger set that broad host range phages can also infect. To test the HRTO, one can ask whether phages with the broader host range are less able to infect the host they share with the narrow host range phage. By focusing on shared hosts, this analysis controls for any host-specific effects that might drive differences in infectivity measurements. Given that few hosts would be shared across modules if Φ were modular, this control and analysis would not be possible if the matrix had a modular structure. Accordingly, the data in Φ provide no evidence of an HRTO because they exhibit consistent trade-ups, whereby phages that are more infective to one bacterial host than another are also likely to infect more hosts (figs. 3, S3).

Adaptation Hot Spots in Lamb Structure (Figs. 4, 5)

Whole-genome sequencing of library strains (and other bacteria generated using the same assay that were not included in the library) revealed that each possessed only a single mutation in genes known to interact with λ (Rajagopala et al. 2011; Blasche et al. 2013; Ragunathan and Vanderpool 2019). All of the mutations were related to resistance mechanisms in either inner-membrane *manYZ* or outer-membrane *lamB* or else were involved in membrane protein regulation (*malT*; tables S1, S2); these mutations have been documented to confer resistance to λ (Meyer et al. 2012). Targeted Sanger sequencing of *lamB* of 50 library strains (table S3) showed that all have *lamB* mutations. To understand the mechanisms by which these mutations might affect both λ resistance and nutrient uptake, we predicted LamB structural changes using the folding algorithm Modeller (https://salilab.org/modeller/). We then searched for correlations between deformations in LamB geometry and phenotypic data by seeking physical differences between the wild-type LamB and its mutants to ascertain whether LamB changes would reflect known λ resistance mechanisms or impact structures responsible for nutrient (maltodextrin) transport. As we now show, some mutations affect structures implicated in both, which helps provide a biophysical basis for some of the trait correlations we observe.

To quantify changes in LamB geometries, we implemented an extension of morphometry (Zelditch et al. 2012) using landmarks provided by the (α carbon) Cα structure of the LamB peptide, which serves as a skeleton of the full protein. These changes were estimated by solving

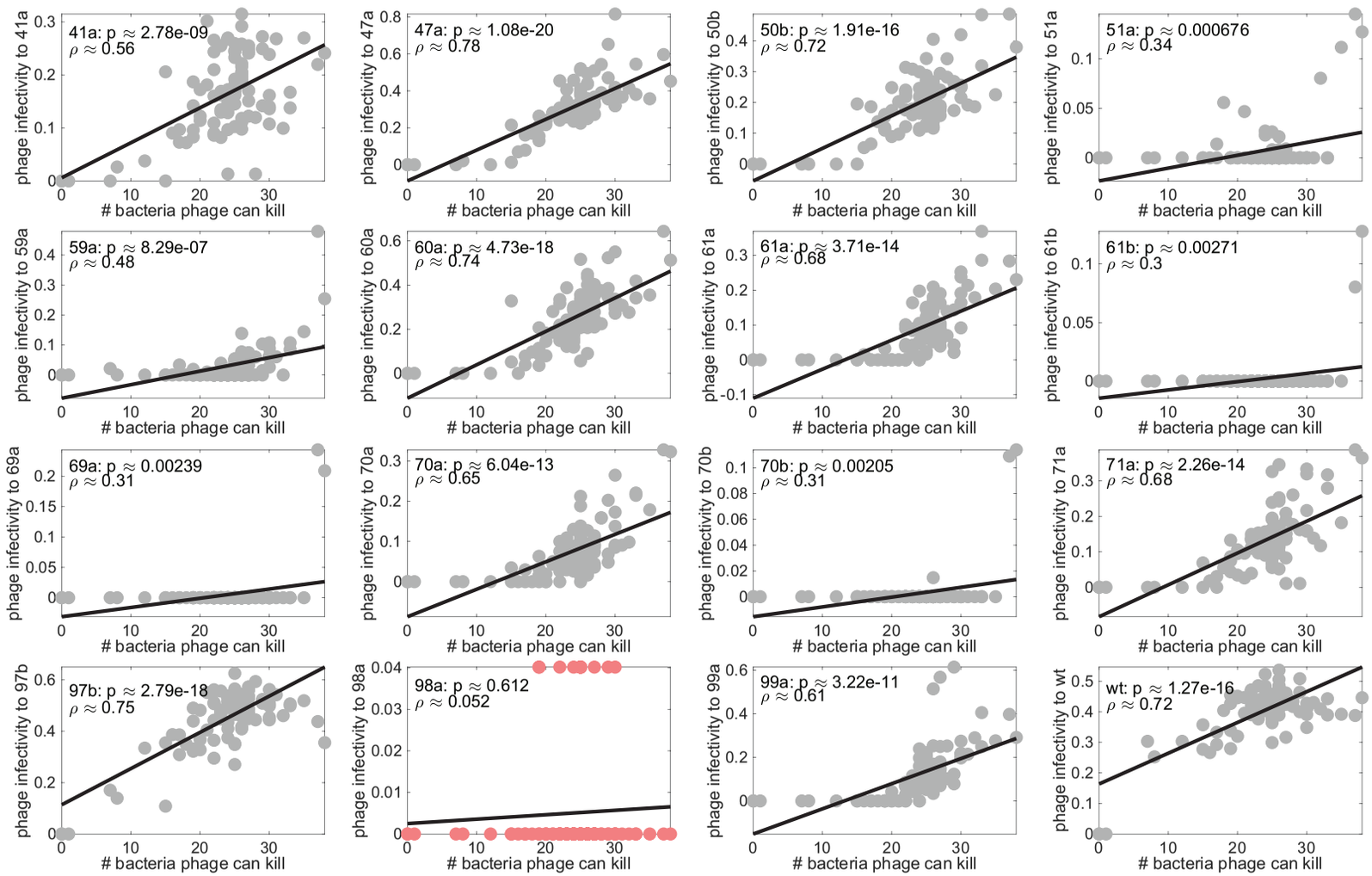

Figure 3: The infectivity matrix in figure 2*A* encodes infectivity-resistance trade-ups (shown are 16 phage-susceptible strains; for all 39 data sets, see fig. S3). These linear regressions demonstrate that the smaller the set of phages that can infect an *Escherichia coli* strain, the less susceptible that strain is to those phages that can infect it. Or said another way, the more susceptible an *E. coli* strain is to each phage, the more phages that can infect it. We deduce this by using Deming regressions between the bacterial infectivity proxies shown in figure 2*A* (a row from that matrix is plotted on the *y*-axis here), and the number of infectious phages in that row (shown on the *x*-axis) are plotted separately for each *E. coli* strain in the library. Thus, for each of the 93 phages—call one X—X can kill a certain number of bacterial strains, and this is the *x*-axis value. Each X also has an imaging-derived numerical infectivity for each bacterial strain; this is the *y*-axis value. When all of the *x*/*y*-axis values are formed into a scatterplot for all 93 phages for one bacterium at a time, Deming regression is then performed. The significance of those regressions are stated as *P* values alongside correlation coefficients, and all but two of 39 correlations (indicated as red points) are significantly positive. Stated ρ values are Pearson correlation coefficients.

a mathematical pattern-matching problem whereby two sets of 3D vectors must be compared and the closest matches found between them (fig. 4*A*, 4*B*). One complication encountered when comparing a mutant LamB structure to its wild type was caused by insertions and deletion mutations in *lamB* that insert or remove amino acids, changing the number of landmarks and confounding which landmarks should be compared by the pattern-matching process. To overcome this, we developed an approach that identified morphological differences between proteins of different sizes, developing an algorithmic heuristic (fig. 4*A*) that extends the Hungarian matching algorithm ("LamB Morphometrics," supplemental PDF). The latter iteratively compares, and rejects, poorly matching substructures of the smaller protein to find better matches within the larger protein.

We applied this algorithm to the wild-type LamB Cα structure, using it as a backbone against which LamB variant structures were compared. The algorithm returns a structure in the lowest dimension of the two being compared that optimally matches a substructure of the largest to the smallest with respect to Euclidean distance. This difference determines structural hot spots, which are those Cα matches contributing more than p% of the total between-protein difference in Euclidean space. Throughout, we made the arbitrary choice of $p = 1$ (black circles in fig. 4*B*; "LamB Morphometrics," supplemental PDF).

First note that the wild-type LamB peptide contains 421 Cα coordinates. To quantify LamB hot spots that correlate with our phenotypes of interest (λ resistance and maltotriose-limited growth), we applied k-means clustering to determine where protein changes clustered for the set of (i) all LamB variant structures with 400 Cα coordinates or more (a set that includes all single-nucleotide polymorphism [SNPs]; table S3) and (ii) only panresistant bacteria (noting there are no *lamB* SNPs in this set; table S3). The number of clusters for sets i and ii was determined by the number of local maxima of a kernel density estimate of the wild type–to–mutant LamB difference data collated for each set of strains.

The resulting hot spots for all library variants are not uniformly distributed throughout LamB but rather are found in the following regions (figs. 5*A*, S4): cluster centers for sets i and ii are found in LamB's outer loops (fig. 5*B*; loops L2, L4, L5, L6, and L9), where loop L2 coincides with a cluster from the set of panresistant hot spots, which is situated at the entry to the so-called greasy slide (fig. S5; loop L2). The latter is a region of aromatic residues along which maltodextrins enter the cell (Schirmer et al. 1995; Van Gelder et al. 2002). Loops L4, L5, L6, and L9 are disjointed from the clusters of panresistant hot spots from set ii (fig. S5), so we speculate that these loops may be associated with lower levels of phage resistance than some, if not all, of the mutations in L2, noting that L2 contains hot-spot clusters of both sets i and ii. In summary, the location of hot spots are consistent with LamB functions that are known to mediate λ resistance and maltotriose uptake.

Reconciling RYTO Theory and CORTO Data: How Nutrient Uptake Reduction Might Increase Absolute Fitness (Figs. 6–9)

Having shown that our bacterial variants have structural alterations implicated in nutrient uptake, we asked whether an RYTO might be found among them because changes in nutrient uptake impact growth rate. The ancestral strain exhibits an RYTO when grown at different resource concentrations, whereby the highest resource concentrations yield the fastest and least efficient growth (Meyer et al. 2015). We therefore tested whether the library derived from that ancestor possessed both within-strain and between-strain RYTOs. Indeed, relating growth rate to population densities per maltotriose supplied (also known as biomass yield) for eight different maltotriose concentrations shows that within-strain RYTOs are present throughout the library (figs. 6*B*, S6). Between-strain growth rate versus yield data do form weak but significant RYTOs at the very lowest maltotriose supply concentrations tested (fig. S7), but in sufficiently rich maltotriose environments variants with greater growth rates also have higher yields (figs. 7*A*, S7); thus, we observe a between-strain rate-yield trade-up, as elsewhere (Reding-Roman et al. 2017).

The analysis culminating in equation (6) provides one insight consistent with this trade-up: given two LamB mutants with different nutrient uptake rates, in an otherwise isogenic background the mutant with slower uptake is predicted to have higher yield. Equation (7) then predicts that slow-uptake strains with elevated yields can also have higher growth rates provided the nutrient supply concentration is high enough; this prediction is consistent with data (figs. 7*A*, S7). Equation (7) also predicts negative between-strain rate-yield correlations at low maltotriose supply, and this is broadly consistent with data (fig. S7). However, the low signal-to-noise ratios present in yield measurements at the low maltotriose concentrations needed to achieve low growth rates means that these negative correlations are weak (fig. S7) and not robust, for example, to outlier removal (scripts for tests are provided in "Testing for consistency of results under different assumptions on data quality," supplemental PDF).

Now, *lamB* missense mutations can increase resistance with little or no impact on nutrient uptake through LamB (Andrews and Fields 2020), and this is relevant because of the CORTO: such mutations leave open the possibility that some library strains might not be subject to the constraints on resistance and fitness that a CORTO would

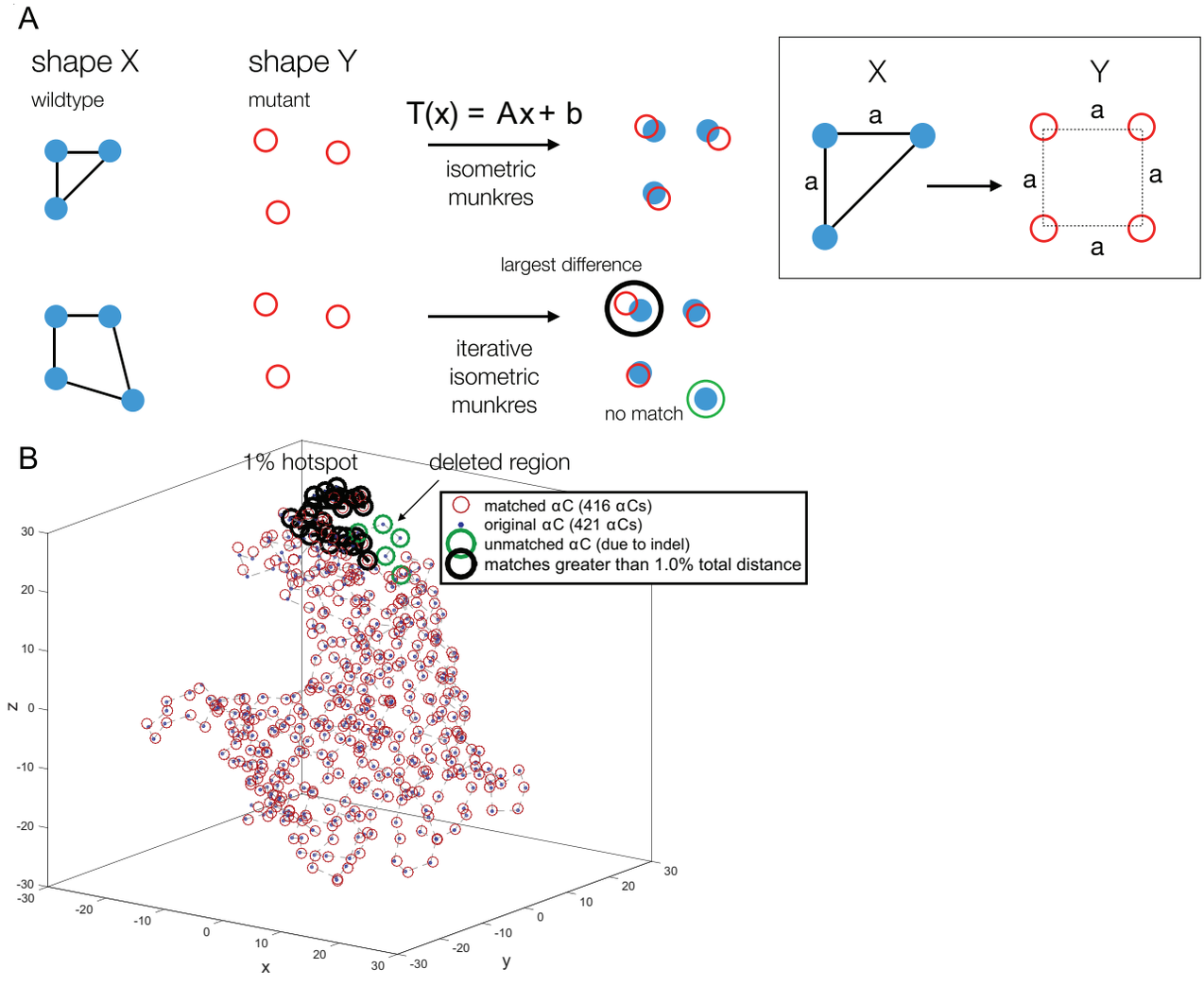

Figure 4: Quantifying the largest geometric changes in mutant LamB structures algorithmically. *A*, Blue points and red circles are spots connected by edges representing two shapes, X and Y, where no common origin is available for both. When X and Y have the same number of nodes, a distance-preserving affine transform, or isometry, T, can be found that places X as close as possible to $T(Y)$, whereafter the transformed nodes in $T(Y)$ can be matched to X using one application of the munkres algorithm. When X and Y have different numbers of nodes, such optimal matches may not be possible (the top right box shows an example where a triangle can be matched optimally into a square of side length a in four different ways due to the rotational symmetry of both). Nevertheless, optimal matches between X-sized subsets of X and Y can be sought iteratively by creating a sequence of isometries whereby subsets of Y (the larger set) are optimally matched to X using munkres ("LamB Morphometrics" in the supplemental PDF provides links to a Matlab implementation). *B*, Shown is a 2D projection of a 3D LamB structure marked with hot spots (black circles) that were obtained by applying the algorithm described in the main text to a mutant LamB Cα structure. Regions lost because of deletion mutations (green circles) are detected, and the largest 1% of differences between matched substructures are highlighted as black circles, denoting a hot spot.

impose. Given this possibility, we asked whether analogies of the rare mutations observed before (Andrews and Fields 2020) might be found within our library.

To address this, we sought a CORTO whereby increased λ resistance would correlate with reductions in some fitness measure, and the response to this is multifaceted. First, there is no correlation between fitness relative to the ancestral strain and λ resistance (fig. 7*C*). Second, all but one bacterial variant has increased λ resistance relative to the ancestor, and while some variants pay a growth rate penalty for this, many do not (fig. 8). Indeed, two strains (labeled 26a and 56a) have different dual benefits in different measures (fig. 8): first, they have higher than ancestral growth rates at all maltotriose

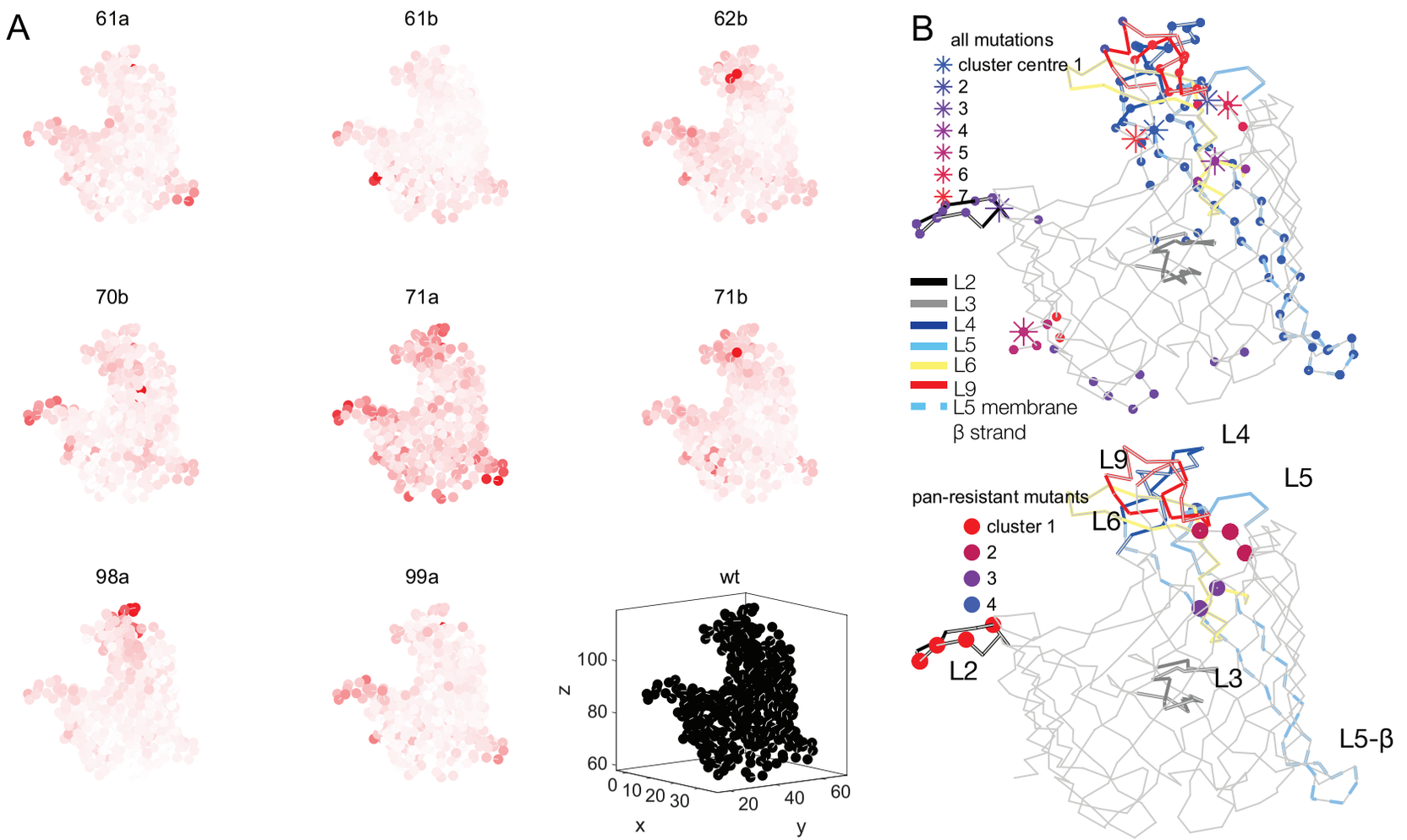

Figure 5: Most clusters of greatest geometric change in LamB occur in surface loops L2–L9. Shown are nine of 42 library bacteria whose LamB has 400 or more Cα coordinates (for the remaining structures not shown here, see fig. S4). Each plot is a 2D projection of a 3D LamB structure (*x*/*y*/*z*-axis labels and scales are shown in the bottom rightmost plot in *A*, which is the wild-type LamB, but axes are omitted for other strains for clarity). *A*, This illustrates hot spots in the deviation between mutant and wild-type LamB for the library strains possessing 400 or more Cα coordinates (table S3). Each LamB change is shown as a heat map superimposed onto the wild-type structure, where white/gray represents no/little structural change and red denotes large changes (i.e., hot spots). The black structure (bottom right corner) is the wild type, shown for reference. *B*, Redder regions in *A* appear to cluster around the entry to the greasy slide (loop L2 in fig. S5) and surface loops. *k*-means clustering demonstrates this quantitatively. *Top*, seven cluster centers (shown as asterisks) were determined by clustering the geometric changes of all observed mutants, where each cluster has been superimposed on LamB. Some are in outer L loops, others are close to a loop. *Bottom*, This shows four analogous cluster centers but determined only for panresistant strains that occur in L2 and close to, but not in, surface loops L4–L6 and L9.

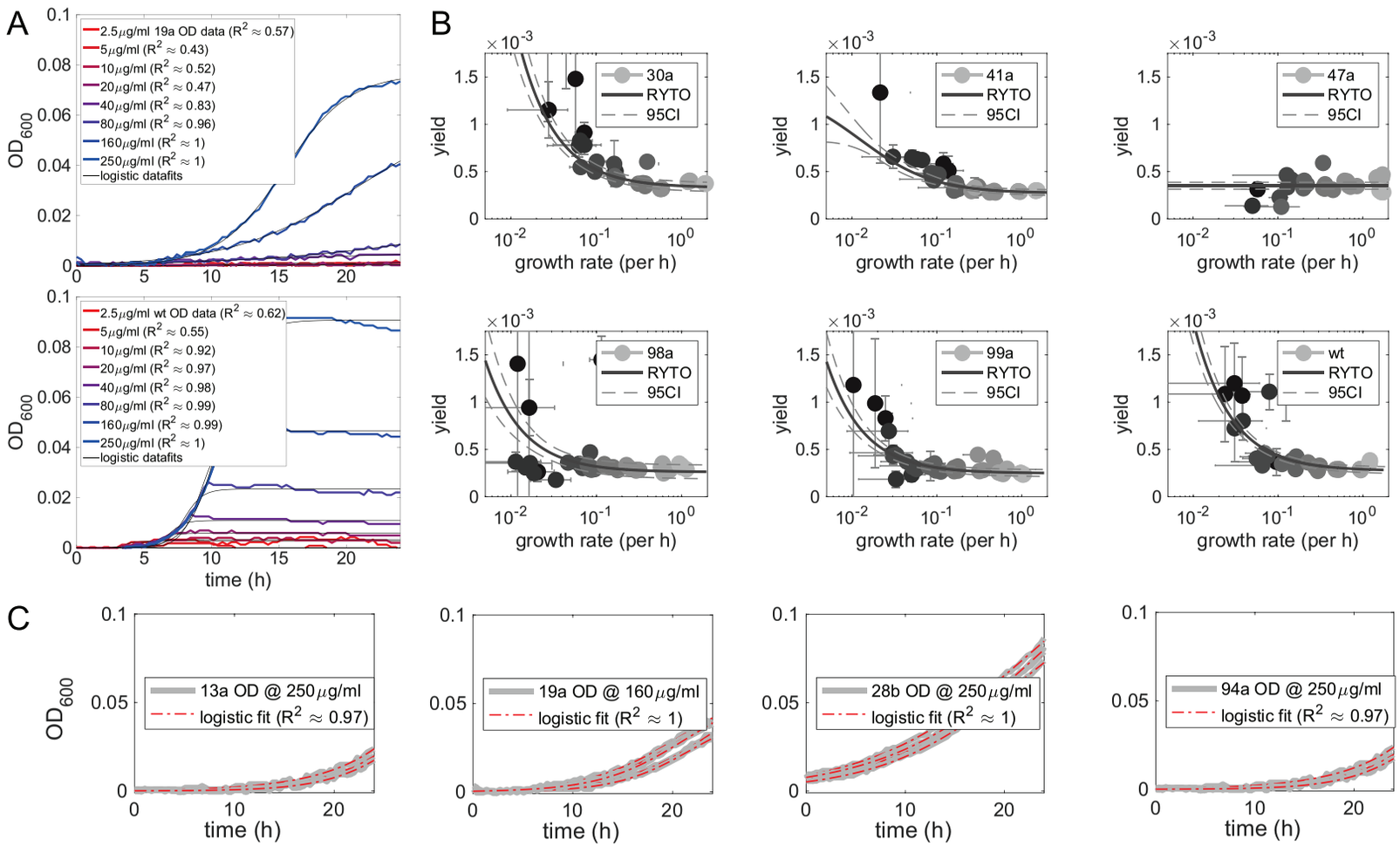

Figure 6: Within-strain rate-yield trade-offs (RYTOs) occur for most library strains (note for *B* and *C*: fig. S6 shows all 46 cultivable strains following transportation between laboratories; shown here is a subset of those). *A*, The RYTO is quantified as follows: *Escherichia coli* is cultured at different maltotriose concentrations, and a logistic model is fitted to population density data (e.g., wild type [*bottom*], strain 19a [*top*]). Logistic growth determines densities up to stationary phase, and biomass yield is estimated as that density divided by the maltotriose concentration supplied; yield could be converted into cells per microgram, but we state it as optical density (OD) at 600 nm per microgram per milliliter. The logistic model also predicts growth rate per hour, and a reduction in yield as maltotriose concentration increases is indicative of an RYTO. Note how the wild type achieves stationary phase but 19a does not, and we therefore cannot quantify an RYTO for the latter. *B*, The resulting (growth rate, yield) data sets from *A* are modeled theoretically ("Bacterial growth phenotypes," supplemental PDF; five replicates, gray regions are 95% confidence intervals [CIs], points are data means, crosshairs show SE), and RYTO models fitted to the data show that many exhibit an RYTO (i.e., a decreasing data fit in each panel; see fig. S6). Exceptions to this are strains for which yield does not decrease as growth rate increases, such as 47a. *C*, Population density dynamics are shown for four slow-growing and highly resistant strains for which yield could not be determined when culturing up to 250 μg/mL (13a, 19a, 28b, 94a). For these strains, OD data show stationary phase was not achieved by 24 h at some maltotriose concentrations, preventing an analysis of their rate-yield relationship because yield cannot be estimated.

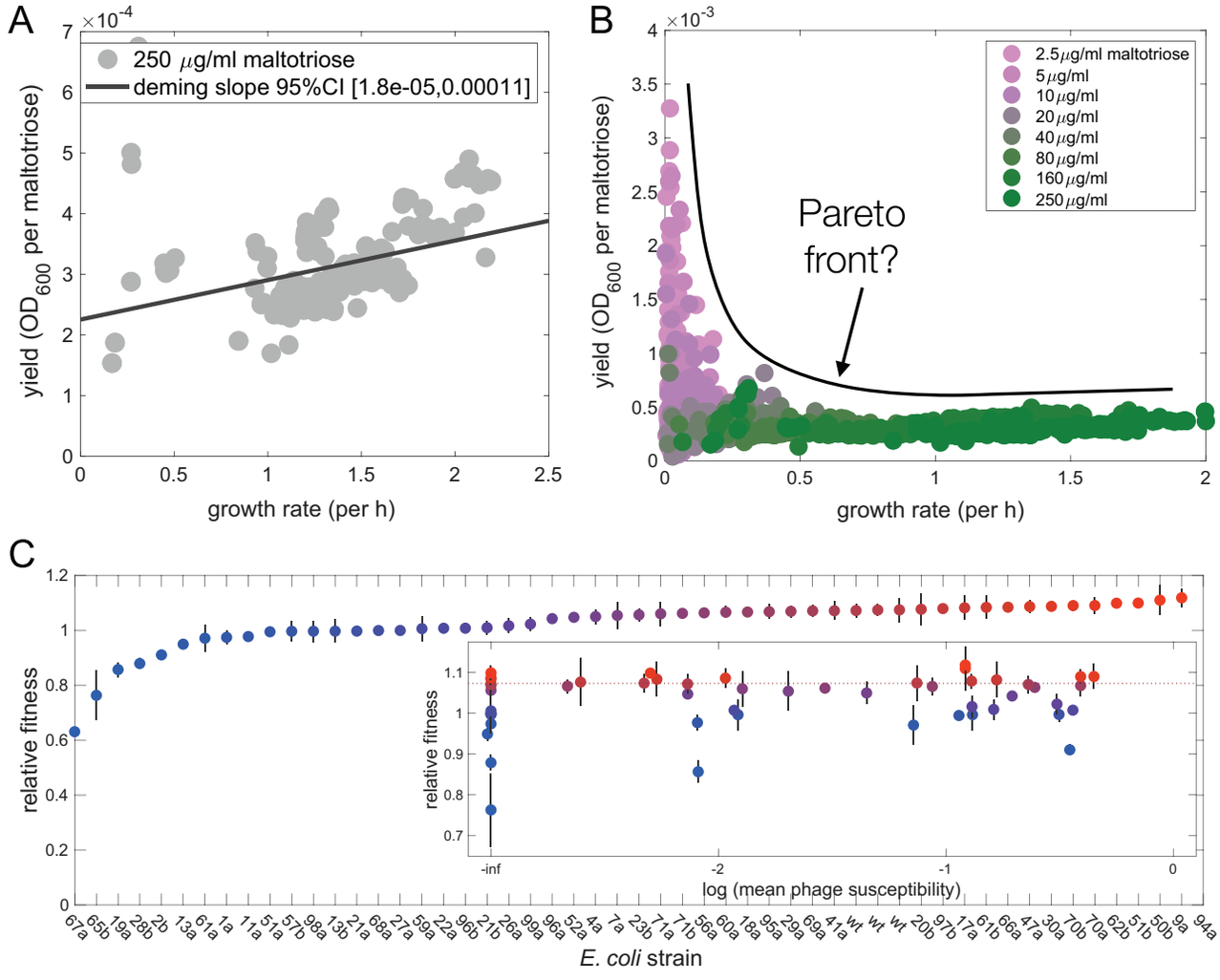

Figure 7: Between-strain data illustrating that growth rate, yield, and relative fitnesses do not exhibit trade-offs (*A* and *B* use data from the 46 strains in fig. S6, while *C* uses the 51 strains from fig. 2). *A*, Significantly positive correlations (i.e., trade-ups) are observed between growth rate and yield in four of eight maltotriose concentrations tested, as illustrated here for 250 μg/mL maltotriose. Not shown here are weak negative correlations (i.e., putative trade-offs) observed at low maltotriose concentrations (see fig. S7). *B*, Placing eight rate-yield data sets from *A* and fig. S7 within common axes indicates a potential Pareto front in (rate, yield) space whereby *Escherichia coli* may be metabolically constrained to lie below that front. A hand-drawn front is shown for illustration. *C*, Relative fitnesses (*y*-axis) were determined with respect to the wild type ($n = 3$ replicates, vertical bars show SE) where the *x*-axis labels denote the bacterial strains tested. The inset is a semilogx scatterplot of λ susceptibility (data from fig. 2) versus relative fitness where the colors—consistent between the main plot and inset—denote one strain. The inset shows that no correlation exists between λ susceptibility and relative fitness; thus, there is no phage resistance cost in terms of relative fitness. Where mean phage susceptibility is zero for a resistant strain, this has been placed at −3 units on the *x*-axis of the inset. CI = confidence interval; OD_{600} = optical density at 600 nm.

concentrations assayed, and they are panphage resistant (figs. 9, 2*A*); second, they have reduced maltotriose half-saturation constants (fig. 8; half-saturation constant K_m is defined in eq. [2]; K_m is determined from data fits detailed in "Bacterial growth phenotypes," supplemental PDF).

Finally, variant 2b is panresistant and has growth rate benefits, but it pays a cost in terms of its decreased half-saturation constant, as, indeed, most other strains do (fig. 8*C*). As a result, there is a significant reduction in median half-saturation constant relative to the wild type ($P \approx 3.1 \times 10^{-6}$, sign test). Thus, analogies of the rare dual-benefit mutations found before (Andrews and Fields 2020) are found here too, albeit as deletions; taken across the strain library, although there is no significant change from the ancestral strain in terms of mean growth rate, there is in terms of half-saturation constant (fig. 8).

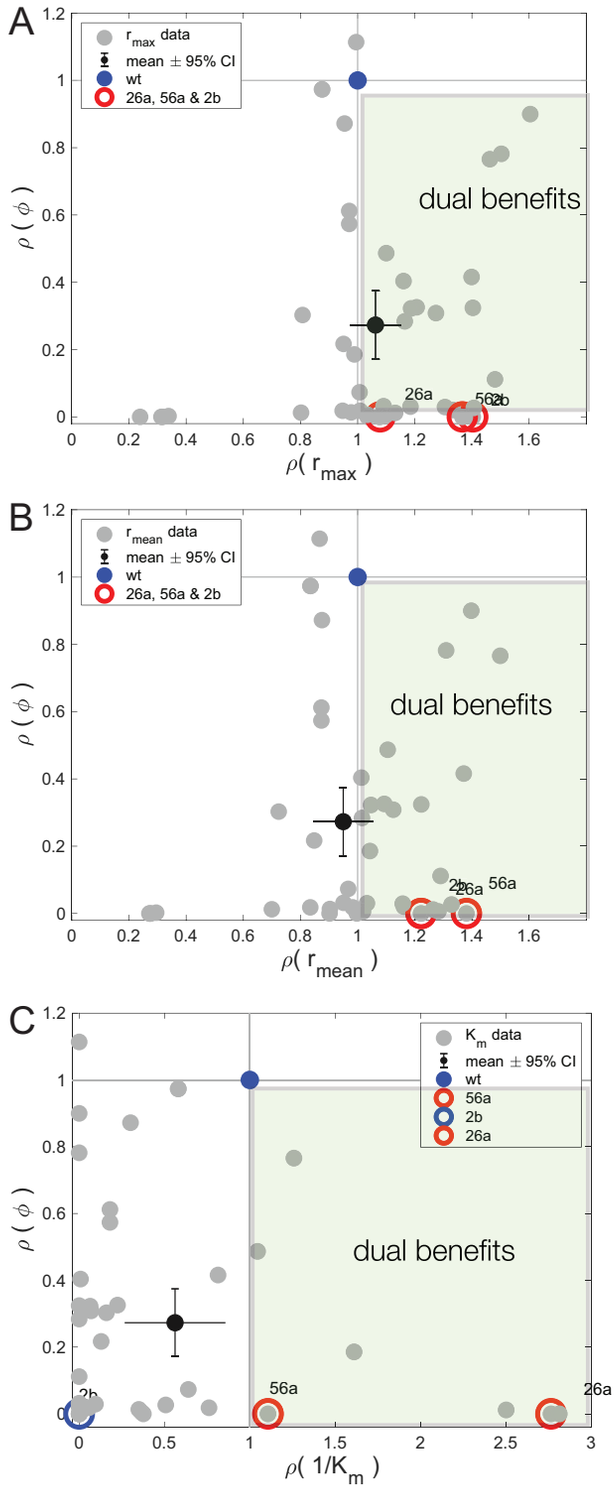

Figure 8: Strains 26a and 56a have improved growth rate, half-saturation constant, and λ resistance relative to the wild type (wt; showing all 46 strains from figs. 6*B*, S6). *A*, This scatterplot shows maximal growth rate (r_{max}; *x*-axis) relative to the wild type versus mean λ susceptibility (ϕ) relative to the wild type (*y*-axis); thus, the wild type (blue point) is unity on both axes. For brevity we have written $\rho(r_{max}) = r_{max}^{mutant}/r_{max}^{wt}$, where r_{max} is growth rate observed at 250 μg/mL maltotriose. Analogously, the mean λ susceptibility relative to the wild type is written $\rho(\phi) = \phi^{mutant}/\phi^{wt}$. These phenotypes are shown for other library strains using a gray point, the library mean is a black point, and crosshairs are estimated 95% confidence intervals (CIs). Importantly, data for strains 26a, 56a, and 2b lie in the regions labeled "dual benefits," where strains have both reduced their λ susceptibility and increased their growth rate relative to the wild type. *B*, This shows the analogous plot to *A* but for mean growth rate (r_{mean}) taken across eight maltotriose concentrations (see "Methods"), where 26a, 56a, and 2b again exhibit dual benefits. *C*, Strains 26a and 56a have improved their half-saturation constant, K_m (see "Bacterial growth phenotypes," supplemental PDF), by reducing it relative to the wild type, but 2b has not. Indeed, most strains have paid a cost for resistance in terms of increased K_m relative to the wild type (the *x*-axis shows the change in $1/K_m$ relative to the wild type).

Discussion

Summary: Evidence For and Against Trade-Offs

We summarize our findings according to three trade-offs: the HRTO, the RYTO, and the CORTO.

i. Data from our image analysis that sought to address the HRTO found no evidence for it. Rather, we found a nested pairwise interaction consistent with a grading of phages according to their infective abilities. There is a debate as to the interpretation of nested pairwise interaction structures in ecology, particularly for mutualistic interactions between species (Payrató-Borràs et al. 2019), but as ours is an antagonistic interaction between two species resulting from a molecular interaction where the analysis is conducted within a species pair, the interpretation of nestedness in figure 2*A* is straightforward: some bacteria resist phages better than others, and some phages attack bacteria more efficiently than others. The consistent relationships in data (figs. 3, S3) suggests that phages can be trained to have superior lytic efficacy by having both broad host range and high infectivity.

ii. We expected to observe an RYTO; we do, and its presence is central to our arguments. Data show that most cells harbor an RYTO whereby growth efficiency decreases as nutrient supply increases (figs. 6*B*, S6). Thus, changes in growth rate due to phage resistance mutations in *lamB* tension two opposing forces. First, nutrient transport rate can decrease whereby intracellular sugars become less abundant, possibly decreasing growth rate. Second, however, increases in biomass yield could result from a reduction in nutrient uptake, thus increasing growth rate. Magnitudes of these respective changes will, in practice, dictate whether growth rates increase or decrease as a result of reductions in nutrient uptake, and theory predicts at least two different possibilities: equation (7) delineates the environment into either case under one particular set of modeling assumptions. Consistent with equation (7), we observe no between-strain RYTO in our

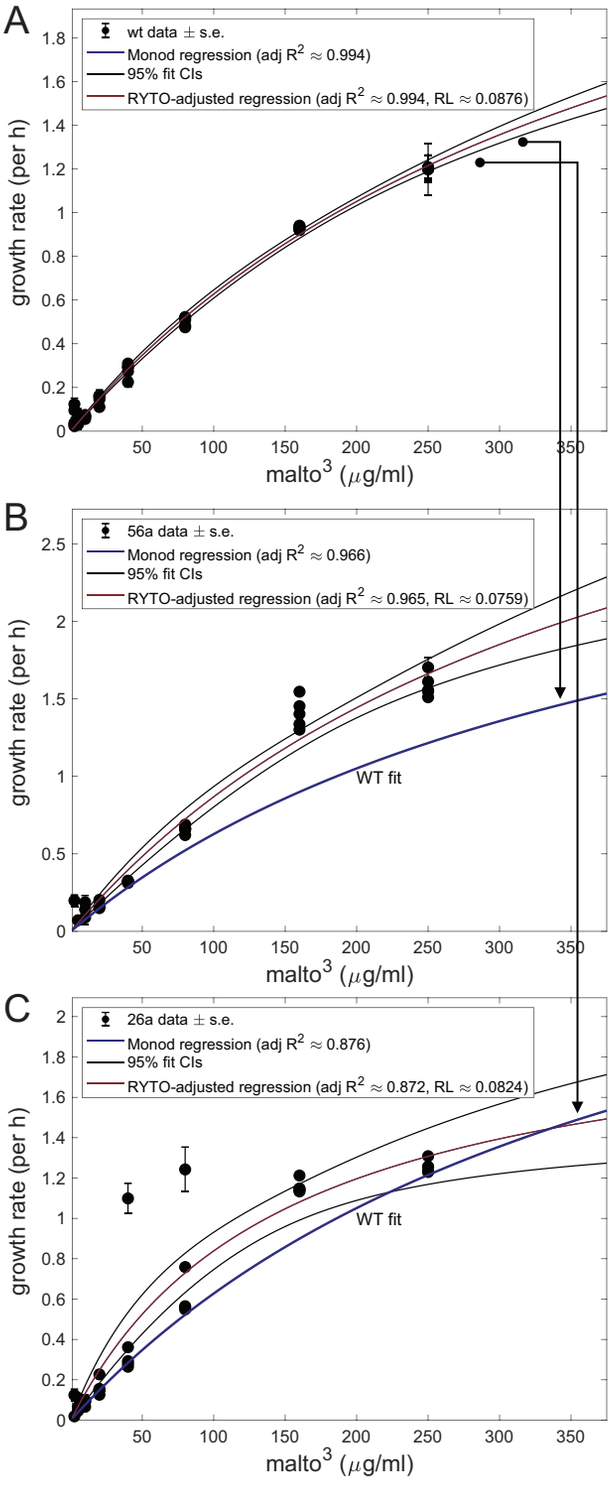

Figure 9: Strains 26a and 56a grow more quickly than the wild type (wt) at all maltotriose concentrations assayed. To see this, note the nonlinear Monod regression (eq. [S1], supplemental PDF) that has been fitted to wild-type growth rate data is shown in *A*, with adjusted R^2 values in the legend. This is repeated in *B* and *C* (see arrows) and the wild-type Monod fit (labeled "WT fit") is placed next to analogous Monod fits of growth rates of 26a and 56a; note how the wild-type fit lies below the confidence intervals (CIs) of the fits of 26a and 56a when the maltotriose concentration is 250 μg/mL or less. Now, because a rate-yield tradeoff (RYTO) is exhibited by these library strains (figs. 6B, S6), an RYTO-adjusted Monod regression based on equation (2) has also been fitted to the growth rate data of the wild type, 26a, and 56a, which assumes that yield decreases with increasing maltotriose supply. These are visually indistinguishable from the standard Monod data fit, which assumes constant yield; consistent with this, none of the relative likelihoods (RLs) between the two types of fit are statistically significant. Section "Bacterial growth phenotypes" in the supplemental PDF details how these fits were performed.

strain library at high maltotriose concentration, and according to equation (7), this is precisely because strains with higher growth rates also have higher biomass yields (figs. 7*A*, S7). Also consistent with equation (7) is the between-strain RYTO found at low maltotriose concentrations (fig. S7), but this is not robust and may be due to the low signal-to-noise ratio in OD measurements at low population densities.

iii. CORTO data exhibit substantial variation between library variants. Some bacteria pay a fitness cost for resistance, but others, unexpectedly, achieve fitness increases alongside resistance increases. In extreme cases, we observe panresistant bacteria with improved growth rate relative to their ancestor that are within approximately 15% of the fastest observed growth rate in the library (fig. 8). Thus, there is no well-defined CORTO in terms of growth rate, but there is one in terms of half-saturation constant (fig. 8), despite strains 26a and 56a not suffering this cost of resistance either.

Although ours is a laboratory study, if clinical phage therapy were to cause both phage resistance and increased bacterial growth rates, it could be catastrophic for a patient, so it is important to understand how this arises. There are at least two mechanisms by which phage resistance evolution could also increase growth rate. One is synergistic pleiotropy: a structural mutation could simultaneously increase the nutrient uptake rate, which could increase growth rate and reduce the binding affinity of the phage. Such mutations have been observed (Andrews and Fields 2020), but this idea is not consistent with our data. First, from the LamB structure analysis, we know mutations deform outer loops and the greasy slide, which are important for sugar translocation (figs. 5, S4). Second, between-strain growth rate increases can come with increased yield (figs. 7*A*, S7). However, growth rate increases come with decreased yield for most individual strains when more maltotriose is supplied (the within-strain RYTO; figs. 6*B*, S6). Thus, the above-described hypothetical synergistic pleiotropy that increases resistance, maltotriose uptake, and therefore growth rate should, in the absence of other mutational changes, decrease yield, yet it need not (figs. 7*A*, S7). Synergistic pleiotropy is therefore unlikely to be the mechanism that explains

our data because here, mutations in LamB must increase phage resistance, growth rate, and yield simultaneously.

One argument consistent with data supporting such "Darwinian demons" that have optimized three traits simultaneously is, again, the analysis supporting equations (6) and (7). Given that we expect a reduction in the maltodextrin uptake rate from the structural analysis, consistent with the reduced growth of 13a, 19a, 28b, and 94a (fig. 6*C*), we argue that the source of this trade-up stems from the phenomenon described by equation (6), whereby increased growth rates result from two processes trading off, one downstream of the other: the transportation of nutrients into the cell, and thereafter the conversion of nutrients into biomass. Equations (6) and (7) (i.e., the condition $Q(S) > 0$) show that phage resistance and reduction in nutrient transportation can increase yield and growth rate provided the maltotriose supply concentration is high enough, as our data require.

Compensatory Mutations

There is another plausible explanation for trade-ups between resistance and fitness: compensatory mutations that overcome the cost of resistance by causing fitness gains could confound the arguments given above. It seems unlikely that 3-day coevolution assays provide enough time for compensatory mutations. However, genomic data provide direct insight into this: 2b's genome reveals just one mutation (table S1), a deletion in *lamB*, despite 2b possessing a trade-up between resistance and growth rate (fig. 8). The LamB structure of 2b has a localized hot spot of greatest geometric change with respect to the wild-type LamB in loop L2 at the entry to the greasy slide; this is situated on the face of the LamB monomers, where the latter binds to form a LamB trimer (Andrews and Fields 2020, their fig. 2, label T; see figure S8). However, we cannot argue that this deletion mutation is entirely cost-free because 2b carries a resistance cost through its increased half-saturation constant (fig. 8).

The genome of 56a exhibits no costs, however, only trade-ups, but it has additional mutations in *rspB* besides one observed in *lamB*. Now, *rspAB* is a starvation-sensing operon that can be upregulated in sugar transport mutants, and it mediates acetate production and increases recombinant protein yield (Jung et al. 2019); there is also evidence that it mediates increases in biomass yield (Weikert et al. 2000). Therefore, 56a may harbor a compensatory mutation in metabolism, but more data are needed to prove this.

Genomes of other library strains reveal additional mutations besides ones for resistance, and an alternative explanation for these "auxiliary" mutations may be passive hitchhiking (table S1). Hitchhikers are likely if strains have elevated mutation rates or if hitchhiking mutations themselves have an elevated rate. There is no evidence that the strains evolved to be mutators, but there is evidence that many of the hitchhikers are common mutations: 73% of these auxiliary mutations are caused by IS element indels that are known to have a high mutation rate in this *Escherichia coli* strain (Consuegra et al. 2021).

We remark that *rbsD* deletion mutations occur frequently in the library in a member of the high-affinity ribose-transport system of *E. coli* (table S1). The latter consists of six proteins encoded in the *rbs* operon (*rbsDACBK* and *R*), and *rbsD* encodes ribose pyranase that is involved in the metabolism of ribose whose overexpression reduces levels of the stress response sigma factor RpoS (Peterson et al. 2019), which itself regulates many genes during starvation (Ferenci 2005). We therefore speculate that the loss of *rbsD* increases RpoS expression, which if true would help cells survive the periods of maltotriose depletion they experience each day while in stationary phase (Notley-McRobb et al. 2002).

Conclusion

Trade-offs are usually studied between two traits held in isolation, and to the best of our knowledge there are few, if any, analyses of interacting trade-offs, although multiple trait interactions are said to be increasingly important for understanding microbial ecosystems (Lindsay et al. 2021). Bacterial fitness is typically a complex function of many genes and traits where interactions are likely, and we have argued that if trait X trades off with Y and trait Y trades off with Z, then X and Z must trade up. Thus, trait interactions can emerge in three-trait data sets that are invisible to two-trait studies.

We reiterate that the logical basis of our main finding is this simple argument. First, phage resistance can be achieved by changes in membrane protein structure that can affect nutrient acquisition. If nutrients enter the bacterium more quickly as a result, then resistance could be cost-free to the host because growth rates could increase. However, if those changes act to slow nutrient uptake, then downstream benefits in metabolism could still accrue and growth rates could increase in any case because of the RYTO, which bestows a benefit of more efficient metabolism when nutrient uptake is reduced. Equation (6) makes this argument precise, and equation (7) provides one theoretical context where this verbal argument applies. Our phenotypic data are consistent with this idea, but the genomes indicate that yet more mechanisms are involved, such as fitness benefits accruing from resistance via mutational pathways that compensate for fitness costs.

A feature we cannot easily address is empirical generalizability: library bacteria and phages were isolated after 3 days of exposure, but suppose we had waited longer—how might that impact our findings? Would trade-ups and trade-offs still be present in the same configurations? Our theory cannot easily address this, nor can our data,

and more highly (i.e., longer) adapted *E. coli*–λ pairs might yet form HRTOs.

To understand how assay duration could be important, imagine that two traits begin by adapting free of any constraints whereby both improve—and thus are positively correlated—before trait limitations are encountered later during the adaptive process. Trade-offs might then only arise as those limits force trait adaptation along a limiting front in trait space (Petrie et al. 2018; Schuech et al. 2019), after sufficient evolutionary time has elapsed. However, for the case of growth rate–resistance trade-offs in our data, we find evidence that trade-ups arise from multiple trade-offs whose interaction has a metabolic and mechanistic basis, not just a correlative one. On that basis, the appearance of trade-ups does not appear to be a case of insufficient time preventing the imposition of physical limits because trade-offs, like the RYTO, are immediately apparent in our data.

For the phage HRTOs, we have not attempted to track down what third (or fourth) trait might trade with host range and infectivity, although we hypothesize that protein stability will (Petrie et al. 2018). Without further investigation, we cannot determine whether the trade-up in λ infectivity is due to evolving far from physical limits or whether other traits may be trading off to produce that particular trade-up. Either way, our data demonstrate that the trade-off between host range and infectivity does not constrain the early stages of coevolution between phage λ and *E. coli*.

Acknowledgments

We thank the National Science Foundation (grant DEB-1934515) for financial support and R. E. Lenski for helpful discussions and support. I.G. was supported financially by a European Research Council (ERC) Consolidator Fellowship (MathModExp: 647292), and R.B. was supported by Engineering and Physical Sciences Research Council (EPSRC) Mathematics for Healthcare UK Hub Co-I, EP/T017856/1. M.H. was supported by R.B.'s EPSRC Healthcare Technologies Impact Fellowship, EP/N033671/1.

Statement of Authorship

J.R.M., R.P.-M., and I.G. were responsible for conceptualization, funding acquisition, and supervision. J.R.M., R.P.-M., and M.H. were responsible for data acquisition. R.P.-M. and R.B. were primarily responsible for data analysis, algorithm development, model analysis, and coding. R.B. wrote the first draft, and J.R.M. and I.G. reviewed and edited it.

Data and Code Availability

All nongenomic data and analysis codes implemented in Matlab R2021b (ver. 9.11.0.1873467, update 3) have been posted to the Dryad Digital Repository (https://doi.org/10.6076/D1R30S; Meyer 2022). Matlab functions are controlled by two master scripts (see readMe.txt and "Descriptions of how to use data and scripts to generate all figures" in the supplemental PDF) that (i) import all raw data and (ii) produce all figures following a single click in the Matlab command window. Scripts are .m files; figures are PDF; data are available in CSV, XLS, and MAT formats; and image data are published as TIF or JPG. Genomic data have been deposited in the ENA (study accession number: PRJEB47962; study unique name: ena-STUDY-UC SAN DIEGO-07-10-2021-01:17:54:061-18).

Literature Cited

Adams, M. 1959. Bacteriophages. Interscience, New York.

Agrawal, A. F., and C. M. Lively. 2002. Infection genetics: gene-for-gene versus matching-alleles models and all points in between. Evolutionary Ecology Research 4:79–90.

Aktipis, C. A., A. M. Boddy, R. A. Gatenby, J. S. Brown, and C. C. Maley. 2013. Life history trade-offs in cancer evolution. Nature Reviews Cancer 13:883–892.

Andersson, D. I., and D. Hughes. 2010. Antibiotic resistance and its cost: is it possible to reverse resistance? Nature Reviews Microbiology 8:260–271.

Andrews, B., and S. Fields. 2020. Distinct patterns of mutational sensitivity for λ resistance and maltodextrin transport in *Escherichia coli* Lamb. Microbial Genomics 6:e000364.

Baquero, F. 2021. Threats of antibiotic resistance: an obliged reappraisal. International Microbiology 24:499–506.

Beardmore, R. E., I. Gudelj, D. A. Lipson, and L. D. Hurst. 2011. Metabolic trade-offs and the maintenance of the fittest and the flattest. Nature 472:342–346.

Blasche, S., S. Wuchty, S. Rajagopala, and P. Uetz. 2013. The protein interaction network of bacteriophage lambda with its host, *Escherichia coli*. Journal of Virology 87:12745–55.

Bohannan, B. J. M., B. Kerr, C. M. Jessup, J. B. Hughes, and G. Sandvik. 2002. Trade-offs and coexistence in microbial microcosms. Antonie Van Leeuwenhoek 81:107–115.

Borghi, E., S. Andreoni, D. Cirasola, V. Ricucci, R. Sciota, and G. Morace. 2014. Antifungal resistance does not necessarily affect *Candida glabrata* fitness. Journal of Chemotherapy 26:32–36.

Borin, J. M., S. Avrani, J. E. Barrick, K. L. Petrie, and J. R. Meyer. 2021. Coevolutionary phage training leads to greater bacterial suppression and delays the evolution of phage resistance. Proceedings of the National Academy of Sciences of the USA 118:e2104592118.

Burmeister, A. R., A. Fortier, C. Roush, A. J. Lessing, R. G. Bender, R. Barahman, R. Grant, B. K. Chan, and P. E. Turner. 2020. Pleiotropy complicates a trade-off between phage resistance and antibiotic resistance. Proceedings of the National Academy of Sciences of the USA 117:11207–11216.

Consuegra, J., J. Gaffé, R. E. Lenski, T. Hindré, J. E. Barrick, O. Tenaillon, and D. Schneider. 2021. Insertion-sequence-mediated mutations both promote and constrain evolvability during a long-term experiment with bacteria. Nature Communications 12:980.

Daegelen, P., F. W. Studier, R. E. Lenski, S. Cure, and J. F. Kim. 2009. Tracing ancestors and relatives of *Escherichia coli* B, and

the derivation of B strains rel606 and bl21(de3). Journal of Molecular Biology 394:634–643.

de Kraker, M. E. A., A. J. Stewardson, and S. Harbarth. 2016. Will 10 million people die a year due to antimicrobial resistance by 2050? PLoS Medicine 13:e1002184.

Ferenci, T. 2005. Maintaining a healthy SPANC balance through regulatory and mutational adaptation. Molecular Microbiology 57:1–8.

Flores, C. O., J. R. Meyer, S. Valverde, L. Farr, and J. S. Weitz. 2011. Statistical structure of host-phage interactions. Proceedings of the National Academy of Sciences of the USA 108:E288–E297.

Flores, C. O., T. Poisot, S. Valverde, and J. S. Weitz. 2016. BiMat: a MATLAB package to facilitate the analysis of bipartite networks. Methods in Ecology and Evolution 7:127–132.

Flores, C. O., S. Valverde, and J. S. Weitz. 2013. Multi-scale structure and geographic drivers of cross-infection within marine bacteria and phages. ISME Journal 7:520–532.

Forde, S. E., R. E. Beardmore, I. Gudelj, S. S. Arkin, J. N. Thompson, and L. D. Hurst. 2008. Understanding the limits to the generalizability of experimental evolutionary models. Nature 455:220–223.

Gudelj, I., R. E. Beardmore, S. S. Arkin, and R. C. MacLean. 2007. Constraints on microbial metabolism drive evolutionary diversification in homogeneous environments. Journal of Evolutionary Biology 20:1882–1889.

Gudelj, I., C. D. Coman, and R. E. Beardmore. 2006. Classifying the role of trade-offs in the evolutionary diversity of pathogens. Proceedings of the Royal Society A 426:97–116.

Hall, A. R., D. De Vos, V.-P. Friman, J.-P. Pirnay, and A. Buckling. 2012. Effects of sequential and simultaneous applications of bacteriophages on populations of *Pseudomonas aeruginosa in vitro* and in wax moth larvae. Applied and Environmental Microbiology 78:5646–5652.

Hofnung, M., A. Jezierska, and C. Braun-Breton. 1976. *lamB* mutations in *E. coli* K12: growth of lambda host range mutants and effect of nonsense suppressors. Molecular and General Genetics 145:207–213.

Interagency Coordination Group on Antimicrobial Resistance. 2019. No time to wait: securing the future from drug-resistant infections. World Health Organization, Geneva.

Jung, H.-M., D.-K. Im, J. H. Lim, G. Y. Jung, and M.-K. Oh. 2019. Metabolic perturbations in mutants of glucose transporters and their applications in metabolite production in *Escherichia coli*. Microbial Cell Factories 18:170.

Keen, E. C. 2014. Tradeoffs in bacteriophage life histories. Bacteriophage 4:e28365.

Kraaijeveld, A. R., and H. C. Godfray. 1997. Trade-off between parasitoid resistance and larval competitive ability in *Drosophila melanogaster*. Nature 389:278–280.

Lenski, R., M. Rose, S. Simpson, and S. Tadler. 1991. Long-term evolution experiment in *Escherichia coli*. I. Adaptation and divergence during 2,000 generations. American Naturalist 138:1315–1341.

Lenski, R. E. 1988. Dynamics of interactions between bacteria and virulent bacteriophage. Pages 1–44 *in* K. C. Marshall, ed. Advances in microbial ecology. Vol. 10. Plenum, New York.

Lindsay, R. J., A. Jepson, L. Butt, P. J. Holder, B. J. Smug, and I. Gudelj. 2021. Would that it were so simple: interactions between multiple traits undermine classical single-trait-based predictions of microbial community function and evolution. Ecology Letters 24:2775–2795.

Lipson, D., R. Monson, S. Schmidt, and M. Weintraub. 2009. The trade-off between growth rate and yield in microbial communities and the consequences for under-snow soil respiration in a high elevation coniferous forest. Biogeochemistry 95:23–35.

MacLean, R. C., and I. Gudelj. 2006. Resource competition and social conflict in experimental populations of yeast. Nature 441:498–501.

Maharjan, R. P., S. Seeto, and T. Ferenci. 2007. Divergence and redundancy of transport and metabolic rate-yield strategies in a single *Escherichia coli* population. Journal of Bacteriology 189:2350–2358.

Mealor, M. A., and M. Boots. 2006. An indirect approach to imply trade-off shapes: population level patterns in resistance suggest a decreasingly costly resistance mechanism in a model insect system. Journal of Evolutionary Biology 19:326–330.

Metz, J. A. J., S. A. H. Geritz, G. Meszena, F. J. A. Jacobs, and J. S. Van Heerwaarden. 1996. Adaptive dynamics: a geometrical study of the consequences of nearly faithful reproduction. Pages 183–231 *in* S. J. van Strien and S. M. Verduyn Lunel, eds. Stochastic and spatial structures of dynamical systems. North Holland, Amsterdam.

Meyer, J. 2022. Data from: Canonical host-pathogen trade-offs subverted by mutations with dual benefits. American Naturalist, Dryad Digital Repository, https://doi.org/10.6076/D1R30S.

Meyer, J. R., D. T. Dobias, J. S. Weitz, J. E. Barrick, R. T. Quick, and R. E. Lenski. 2012. Repeatability and contingency in the evolution of a key innovation in phage lambda. Science 335:428–432.

Meyer, J. R., I. Gudelj, and R. Beardmore. 2015. Biophysical mechanisms that maintain biodiversity through trade-offs. Nature Communications 6:6278.

Meyer, J. R., and R. E. Lenski. 2019. Subtle environmental differences have cascading effects on the ecology and evolution of a model microbial community. Pages 273–288 *in* Evolution in action: past, present and future. Springer, Cham.

Miedzybrodzki, R., J. Borysowski, B. Weber-Dabrowska, W. Fortuna, S. Letkiewicz, K. Szufnarowski, Z. Pawelczyk, et al. 2012. Clinical aspects of phage therapy. Advances in Virus Research 83:73–121.

Molenaar, D., R. van Berlo, D. de Ridder, and B. Teusink. 2009. Shifts in growth strategies reflect tradeoffs in cellular economics. Molecular Systems Biology 5:323.

Notley-McRobb, L., T. King, and T. Ferenci. 2002. *rpoS* mutations and loss of general stress resistance in *Escherichia coli* populations as a consequence of conflict between competing stress responses. Journal of Bacteriology 184:806–811.

Novak, M., T. Pfeiffer, R. E. Lenski, U. Sauer, and S. Bonhoeffer. 2006. Experimental tests for an evolutionary trade-off between growth rate and yield in *E. coli*. American Naturalist 168:242–251.

Payrató-Borràs, C., L. Hernández, and Y. Moreno. 2019. Breaking the spell of nestedness: the entropic origin of nestedness in mutualistic systems. Physical Review X 9:031024.

Peterson, C., S. Dorlean, D. Parsons, T. Tran, and A. Dey. 2019. Regulation of RpoS by RbsD in *Escherichia coli*. Biochemistry and Molecular Biology 33:778.13.

Petrie, K. L., N. D. Palmer, D. T. Johnson, S. J. Medina, S. J. Yan, V. Li, A. R. Burmeister, and J. R. Meyer. 2018. Destabilizing mutations encode nongenetic variation that drives evolutionary innovation. Science 359:1542–1545.

Petrovic Fabijan, A., R. C. Y. Lin, J. Ho, S. Maddocks, N. L. Ben Zakour, J. R. Iredell, A. Khalid, et al. 2020. Safety of bacteriophage

therapy in severe *Staphylococcus aureus* infection. Nature Microbiology 5:465–472.

Pfeiffer, T., and S. Bonhoeffer. 2002. Evolutionary consequences of tradeoffs between yield and rate of ATP production. Zeitschrift für Physikalische Chemie 216:51–63.

Poelwijk, F. J., M. G. J. de Vos, and S. J. Tans. 2011. Tradeoffs and optimality in the evolution of gene regulation. Cell 146:462–470.

Ragunathan, P. T., and C. K. Vanderpool. 2019. Cryptic-prophage-encoded small protein DicB protects *Escherichia coli* from phage infection by inhibiting inner membrane receptor proteins. Journal of Bacteriology 201:e00475-19.

Rajagopala, S. V., S. Casjens, and P. Uetz. 2011. The protein interaction map of bacteriophage lambda. BMC Microbiology 11:213.

Reding-Roman, C., M. Hewlett, S. Duxbury, F. Gori, I. Gudelj, and R. Beardmore. 2017. The unconstrained evolution of fast and efficient antibiotic-resistant bacterial genomes. Nature Ecology and Evolution 1:0050.

Rohde, C., G. Resch, J.-P. Pirnay, B. G. Blasdel, L. Debarbieux, D. Gelman, A. Gorski, et al. 2018. Expert opinion on three phage therapy related topics: bacterial phage resistance, phage training and prophages in bacterial production strains. Viruses 10: 178.

Sambrook, J., and D. W. Russell. 2001. Molecular cloning: a laboratory manual. 3rd ed. Cold Spring Harbor Laboratory Press, Cold Spring Harbor, NY.

Sanchez, C. 2011. Phage resistance comes at a cost. Nature Reviews Microbiology 9:398–399.

Sandegren, L., and D. I. Andersson. 2009. Bacterial gene amplification: implications for the evolution of antibiotic resistance. Nature Reviews Microbiology 7:578–588.

Schirmer, T., T. Keller, Y. Wang, and J. Rosenbusch. 1995. Structural basis for sugar translocation through maltoporin channels at 3.1 Å resolution. Science 267:512–514.

Schuech, R., T. Hoehfurtner, D. J. Smith, and S. Humphries. 2019. Motile curved bacteria are pareto-optimal. Proceedings of the National Academy of Sciences of the USA 116:14440–14447.

Spanakis, E., and M. T. Horne. 1987. Co-adaptation of *Escherichia coli* and coliphage *λvir* in continuous culture. Journal of General Microbiology 133:353–360.

Summers, W. C. 2001. Bacteriophage therapy. Annual Review of Microbiology 55:437–451.

Thirion, J. P., and M. Hofnung. 1972. On some genetic aspects of phage λ resistance in *E. coli* K12. Genetics 71:207–216.

Travisano, M., J. A. Mongold, A. F. Bennett, and R. E. Lenski. 1995. Experimental tests of the roles of adaptation, chance, and history in evolution. Science 267:87–90.

Van Gelder, P., F. Dumas, I. Bartoldus, N. Saint, A. Prilipov, M. Winterhalter, Y. Wang, et al. 2002. Sugar transport through maltoporin of *Escherichia coli*: role of the greasy slide. Journal of Bacteriology 184: 2994–2999.

Weikert, C., F. Canonaco, U. Sauer, and J. E. Bailey. 2000. Co-overexpression of RspAB improves recombinant protein production in *Escherichia coli*. Metabolic Engineering 2:293–299.

Weitz, J. S., H. Hartman, and S. A. Levin. 2005. Coevolutionary arms races between bacteria and bacteriophage. Proceedings of the National Academy of Sciences of the USA 102:9535–9540.

Weitz, J. S., T. Poisot, J. R. Meyer, C. O. Flores, S. Valverde, M. B. Sullivan, and M. E. Hochberg. 2013. Phage-bacteria infection networks. Trends in Microbiology 21:82–91.

Werts, C., V. Michel, M. Hofnung, and A. Charbit. 1994. Adsorption of bacteriophage lambda on the LamB protein of *Escherichia coli* K-12: point mutations in gene J of lambda responsible for extended host range. Journal of Bacteriology 176:941–947.

Zelditch, M., D. Swiderski, and H. D. Sheets. 2012. Geometric morphometrics for biologists: a primer. 2nd ed. Academic Press, Cambridge, MA.

Associate Editor: Elizabeth A. Ostrowski
Editor: Daniel I. Bolnick

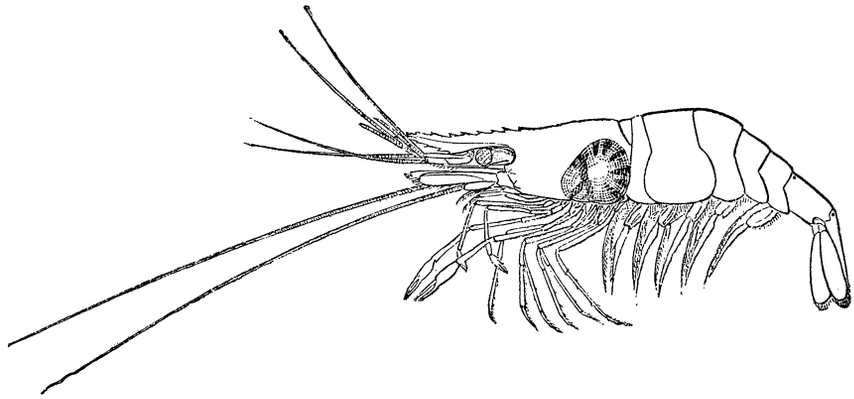

"The common prawn (*Palæmonetes vulgaris* Stm.) with its parasite." From "A Singular Parasitic Isopod Crustacean and Some of its Developmental Stages" by Carl F. Gissler (*The American Naturalist*, 1882, 16:6–12).